CHAPTER 9

TIME-RESOLVED STUDIES

DENNIS M. MILLS

Cornell High Energy Source (CHESS), Cornell University, Ithaca, NY 14853 and Advanced Photon Source (APS), Argonne National Laboratory, Argonne, IL 60439

Contents

Copy for Author's Information

Handbook on Synchrotron Radiation, Vol. 3, edited by G. Brown and D.E. Moncton

1. Introduction

When new or more powerful probes become available that offer both shorter data-collection times and the opportunity to apply innovative approaches to established techniques, it is natural that investigators consider the feasibility of exploring the kinetics of time-evolving systems. This stimulating area of research not only can lead to insights into the metastable or excited states that a system may populate on its way to a ground state, but can also lead to a better understanding of that final state. Synchrotron radiation, with its unique properties, offers just such a tool to extend X-ray measurements from the static to the time-resolved regime. The most straightforward application of synchrotron radiation to the study of transient phenomena is directly through the possibility of decreased data-collection times via the enormous increase in flux over that of a laboratory X-ray system. Even further increases in intensity can be obtained through the use of novel X-ray optical devices. Wide-bandpass monochromators, e.g., that utilize the continuous spectral distribution of synchrotron radiation, can increase flux on the sample several orders of magnitude over conventional X-ray optical systems thereby allowing a further shortening of the data-collection time.

Another approach that uses the continuous spectral nature of synchrotron radiation to decrease data-collection times is the "parallel data collection" method. Using this technique, intensities as a function of X-ray energy are recorded simultaneously for all energies rather than sequentially recording data at each energy, allowing for a dramatic decrease in the data-collection time.

Perhaps the most exciting advances in time-resolved X-ray studies will be made by those methods that exploit the pulsed nature of the radiation emitted from storage rings. Pulsed techniques have had an enormous impact in the study of the temporal evolution of transient phenomena. The extension from continuous to modulated sources for use in time-resolved work has been carried over in a host of fields that use both pulsed particle and pulsed electromagnetic beams. For example, modulated electron beams in scanning electron microscopes have been used in stroboscopic studies of surface acoustic waves and, recently, the first picosecond-resolution electron-diffraction experiments have been shown to be feasible. Likewise, pulsed neutron beams, although used primarily for the energy analysis of inelastic-scattering measurements, have been used to perform time-resolved diffraction studies. With regard to studies with electromagnetic radiation, pulsed sources have proven to be an incisive tool, perhaps the most exciting and useful device being the laser. It is interesting to note that many of the properties that have made pulsed dye lasers such an exciting tool for optical transient studies, high-repetition rate, short-pulse duration and spectral tunability, are similar to the properties of X-radiation emitted from storage-ring sources.

The unique temporal properties of synchrotron radiation have not gone unnoticed by synchrotron-radiation users, particularly those investigators working in the visible and ultra-violet region of the spectrum. Several excellent review articles have been written discussing techniques and experiments that have been performed in this wavelength regime (Monahan and Rehn 1978, Munro and Sabersky 1980, Munro and Schwenter 1983). With that in mind, the scope of this chapter will be limited to studies that utilize the X-ray portion of the spectrum. [See Mills (1984), Gruner (1987) for short reviews on time-resolved X-ray synchrotron-radiation research.]

The extraordinary gains that can be realized in brightness and tunability when going from a laboratory X-ray generator to a storage-ring source of X-rays have been summarized by other authors in earlier volumes of this series. What is perhaps not as well appreciated are the temporal properties of the emitted radiation and it is, therefore, quite useful to review those characteristics.

2. The temporal properties of synchrotron radiation

2.1. Pulse duration

The pulsed nature of the emitted radiation is due to the natural bunching of the circulating particles (positrons or electrons) by the radio frequency (RF) cavity that is used to replenish energy to the particle beam which lost energy through the emission of synchrotron radiation. To see why this bunching occurs, consider a particle that, for a given magnetic-field configuration of the storage ring, has the correct energy E_0 to travel along the nominally correct orbit. This particle follows a trajectory of pathlength L_0 and has an orbital period given by $T_0 = L_0/c$, where c is the speed of light. For the same magnetic-field geometry, a particle with a slightly different energy than the nominal energy, $E = E_0 + \Delta E$, will travel in an orbit that has a different circumference, $L = L_0 + \Delta L$. The magnitude of the pathlength difference is a function only of the strength and configuration of magnetic guide-field. The relative pathlength difference is related to the relative energy deviation through the dimensionless parameter α, i.e., $(\Delta L/L_0) = \alpha(\Delta E/E_0)$. It is important to realize that α, often called the momentum compaction factor, is a number that is always positive for storage rings so that a positive energy increase results in a larger orbital circumference.

If a particle with energy E_0 passes through a radio-frequency cavity at just the right time so that it gains the same amount of energy from the cavity that it lost on its last orbit from synchroton radiation (U_{SR}), it is called a synchronous particle. Consider now another particle, also with energy E_0, that arrives at the RF cavity at a slightly later time than the synchronous particle (shown as the open square in fig. 1). This particle receives an amount of energy differing by ε from its synchrotron-radiation loss. On the negative slope of the RF voltage plot, a late particle receives slightly less energy than the synchronous particle, and hence will take a slightly shorter trajectory around the ring (i.e., the particle will spiral inwards). The concomitant decrease in the amount of time required to circumnavigate the ring will, therefore, cause this particle to arrive less late on the next orbit. With every additional pass, it will gain a bit more

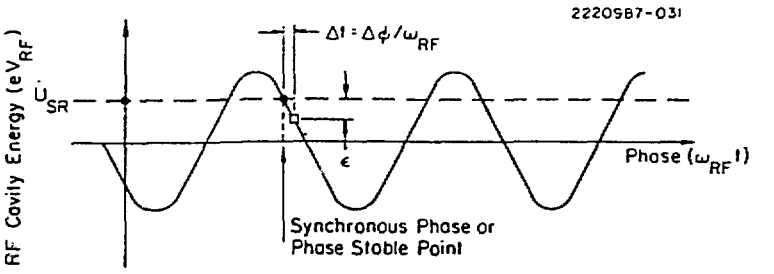

Fig. 1. The radio-frequency (RF) cavity energy as a function of phase or time. A particle arriving at just the right time to receive the same amount of energy it has lost from synchrotron-radiation emission on the last orbit (U_{SR}) is called a synchronous particle. On the negative slope of the RF energy curve, a particle arriving a time Δt latter receives less energy, ($U_{SR} - \varepsilon$) than those arriving at the synchronous phase while those arriving early would receive more.

energy than on the previous circuit, and slowly will begin to increase its orbital circumference and approach the orbit of the synchronous particle. A similar argument can be made for the particle arriving at some time earlier than the synchronous particle, only in this case it receives more energy than was lost through synchrotron radiation and spirals outwards resulting in a longer orbital period, and arriving less early on the next orbit. This self-regulatory process of damping of energy deviations will continue and the energy of the particle will eventually converge on the nominally correct energy. The position on the RF power curve where this natural shepherding of particles occurs is called the phase stable or synchronous phase point. Note that the phase stable point lies on that part of the RF power curve where the slope is negative so there is only one phase stable point per RF cycle.

The oscillations in the energy of the particles about the nominally correct energy described above are called synchrotron oscillations. With the simplified formulation given above, the entire packet of particles would eventually coalesce about the synchronous electron. In a real storage ring, this model will breakdown because the energy losses of the particles through synchrotron-radiation emission are not continuous as in our simplistic model, but are quantized. The discrete emission of quanta causes an instantaneous change in the energy of the particle disturbing slightly the trajectory of that particle. Because the emission of each quantum is statistically independent, the net result on the particle of many of these random disturbances is a growing change in energy as a function of time, causing the ensemble of particles to increase in size. The balance between the increase in energy spread due to quantum emission, and the energy damping mechanism described above determines the length of the particle packet.

In a non-interacting model (i.e., the effects of the environment of the beam are ignored), the bunch profile is expected to be Gaussian. The expression for the bunch length of a low particle-density packet has been derived by several authors (Sands 1970, 1971, Krinsky et al. 1983) and the details of this calculation will be omitted here. However, it is informative to write the expression for the bunch length in terms of the

accelerator parameters to see how these parameters influence the X-ray pulse duration. For an isomagnetic lattice (i.e., all dipoles are of equal strength), the bunch length can be written as

$$\sigma_Z = K_1 \frac{\alpha\gamma}{\Omega_s}\left(\frac{1}{J_E\rho_0}\right)^{1/2},$$

where γ is the ratio of total particle energy to rest-mass energy, Ω_s the synchrotron oscillation frequency, ρ_0 the magnetic radius and J_E the energy-damping partition number. In the isomagnetic approximation, J_E can be written as $J_E = 2 + \alpha R_0/\rho_0$ and is approximate to 2. (R_0 is defined as $L_0/2\pi$.) K_1 is a numerical constant equal to 186 $m^{3/2}\,s^{-1}$. This equation can be recast more in terms of the physical parameters of the storage ring by replacing the angular synchrotron oscillation frequency, Ω_s, by $(\alpha e\dot{V}_0/T_0E_0)^{1/2}$ where $\dot{V}_0$ is the time derivative of the RF voltage evaluated at the synchronous phase, ϕ_0. We can then write

$$\sigma_Z(\mathrm{m}) = K_2\left(\frac{\alpha E_0^3 T_0}{J_E e\dot{V}_0\rho_0}\right)^{1/2},$$

where now K_2 is equal to 3.64×10^5 $m^{3/2}\,s^{-1}\,GeV^{-1}$. To get an estimate of a typical bunch length, let us assume that the RF voltage is sinusoidal, i.e.,

$$V(t) = V_{RF}\sin[2\pi\nu_{RF}(t - t_0)],$$

$$\dot{V}_0 = 2\pi\nu_{RF}V_{RF}\cos\phi_0.$$

Taking $J_E \simeq 2$, $\phi_0 \simeq 45°$ and typical running parameters for the Cornell Electron Storage Ring (CESR): $\alpha = 0.014$, $E_0 = 5.2$ GeV, $T_0 = 2.56 \times 10^{-6}$ s, $\rho_0 = 88$ m, $\nu_{RF} = 500$ MHz, $eV_{RF} = 4.5$ MeV; the calculated one-sigma bunch-length value is 1.95 cm corresponding to a one-sigma pulse duration of 65 ps. A more detailed calculation of the bunch length of CESR when taking into account the actual magnetic lattice yields a value of 68 ps (Blum et al. 1983).

This expression for the bunch length is valid only when the density of particles is low. As the number of particles per bunch is increased, bunch lengthening can occur (Wilson et al. 1979, Photon Factory Activity Report 1984/1985, Garvey 1984); this effect is generally attributed to the collective effects of the beam with its environment, namely the vacuum chamber and any other components (RF cavities, crotches, etc.) associated with the beam-transport system.

The measurement of bunch lengths in storage rings can be made with a variety of instruments depending on the actual timescales involved. Photomultiplier tubes (Lopez-Delgado et al. 1976), image dissector tubes (Brown et al. 1983a), X-ray photodiodes (Wilson et al. 1979, Kania et al. 1986), X-ray sensitive photoconducting devices (Blum et al. 1983), and streak cameras (Monahan et al. 1979, Photon Factory Activity Report 1983/1984) have been employed to measure this important temporal parameter. The bunch length at CHESS has been measured with a high-speed X-ray sensitive photoconducting detector (Blum et al. 1983, Auston et al. 1983) and sampling oscilloscope (fig. 2). These photoconducting devices are extremely fast with measured response times of 2.5 ps in the visible region of the spectrum. With this

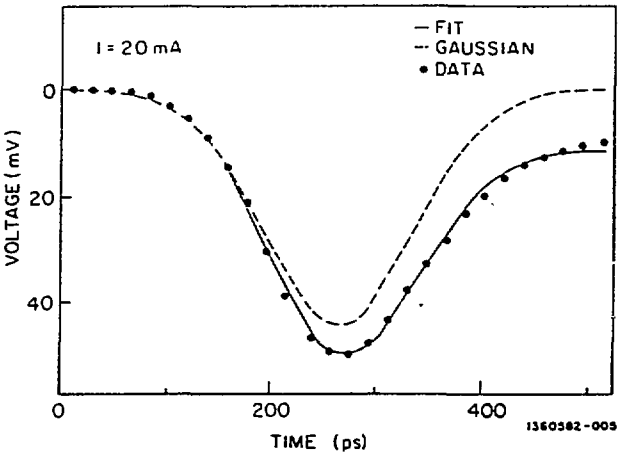

Fig. 2. Measurement of the bunch length at the Cornell Electron Storage Ring (CESR). (a) A schematic of the electrode geometry of the photoconductor used in the measurement. The cross-hatched region denotes the active area of the device. (b) The sampling oscilloscope output of the photoconducting device when put into the CHESS X-ray beam horizontal scale is 100 psec per division). (c) Digitized output of the device and curves assuming the output proportional to beam shape (dashed lines) and the output proportional to the beam shape plus a term proportional to the integral of the beam shape (solid line) (Blum et al. 1983).

device, the bunch duration at CHESS running at 5.17 GeV and 20 mA was measured to be 72 ps, in good agreement with the 68 ps value quoted earlier.

When using sampling methods such as in the measurement discussed above, the resultant pulse profile is the average of many (perhaps thousands) of passes of that pulse; therefore, such methods are incapable of observing variations in the pulse shape from one pass to the next. Although slow oscillations ($\leqslant 100$ Hz) may be observable, high-frequency oscillations and pulse-to-pulse shape variations can only be observed with X-ray streak cameras, by far the most informative devices used to measure the bunch lengths. During a machine-physics study period to look at problems associated with very short bunch lengths at the Stanford Positron–Electron Storage Ring, both symmetric and antisymmetric oscillations were observed from sequential one-shot streak-camera photographs. Not only have X-ray streak-camera measurements revealed that the bunch can oscillate or breathe, but that the bunch itself may not remain Gaussian and have high-frequency structure within the bunch (Munro and Schwenter 1983, Mills 1984). Such factors could be of importance if accurate measurements are attempted with temporal resolution commensurate with that of the pulse duration. Unfortunately, however, accurate measurements of the pulse profile have been made at few storage-ring sources.

Geometrical effects may lead to a broadening of the observed pulse length. These effects are small compared to the pulse durations of all existing machines. However, they may become appreciable if bunch lengths can be made extremely small, as may be the case in dedicated machines now being considered for construction. The slight

path-length difference ΔP between the straight line trajectory of the photons and the curved trajectory of the particle as it is bent by the dipole magnets can cause an apparent increase in pulse duration. To second order in the angular horizontal viewing aperture δ this is equal to (fig. 3a)

$$\Delta P = (L' + S) - (L_1 + L_2) = \tfrac{1}{2}L^1\delta^2 = \tfrac{1}{2}D\delta,$$

where D is the horizontal detector aperture and δ the horizontal angle subtended. Even with a somewhat large aperture of 10 mrad at 20 m from the source, the observed increase in pulse duration would only be 3.3 ps.

Insertion devices can also produce an apparent pulse lengthening due to the difference in path length between the emitted X-rays and the sinuous trajectory that the radiating particle follows through such a device (fig. 3b). The path-length difference in this case is

$$\Delta P = \frac{NK^2}{4\gamma^2} + O\left(\frac{K}{\gamma}\right)^4,$$

with N being the number of magnetic periods in the insertion device, K the magnetic-magnetic-field strength parameter [$K = 0.093B(\mathrm{kG})\lambda_{in}$ (cm), where λ_{in} is the magnetic

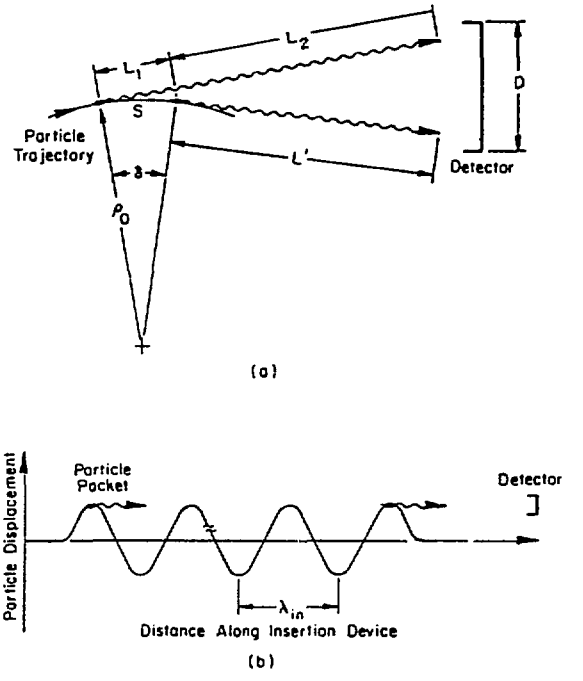

Fig. 3. Geometrical broadening of the observed pulse duration can occur from (a) dipole magnet sources and (b) insertion devices sources because of the path-length difference between the curved trajectory of the particles and emitted photons.

of the insertion device). Again, the effects are small. Even for a high-field wiggler ($K = 100$) with 100 periods inserted in a low-energy machine (1 GeV), this corresponds to a pulse broadening of only 2.1 ps.

2.2. Interpulse period

If a particle has to receive energy from the RF cavity on every orbit, the RF frequency must be some multiple of the orbital frequency of the particle, i.e.,

$$\nu_{RF} = n(1/T_0) = n\nu_{\text{orbital}},$$

where n is an integer called the harmonic number. Since there is one phase stable point at every RF cycle, this implies that there are n stable orbital positions or RF "buckets" in which the particles can circulate around the storage ring. The number and configuration of filled RF buckets determines the interpulse period of the X-ray bursts. The filled configuration can be a function of a number of considerations including whether the storage ring is being run for high-energy physics research or whether it is a dedicated synchrotron-radiation source. Typical repetition rates for large storage rings are from 0.5 to 100 MHz (table 1). The time between X-ray bursts has not necessarily to be uniform, again depending on the specific configuration of the filled RF buckets.

The orbital period of the ring is probably one of the better-known temporal parameters of the machine. The stability of the orbital frequency is determined by the stability of the clock driving the RF accelerating system. The precision of the quartz oscillator clocks used in this application are typically 10^{-7}–10^{-8}, resulting in a jitter of the orbital period that can be less than a picosecond.

2.3. Temporal purity

Depending on the type of experiment to be performed, the temporal "purity" of the beam (the "darkness" of the periods between pulses) may be important to insure success. Measurements of the single-bunch purity at the SRS at Daresbury showed that spill into adjacent RF buckets could be kept to less than 0.2% of the particle number of the targeted bucket during the filling process (Brown et al. 1983b). Because of the small size of these satellite bunches ($< 1\%$), the introduction of a large counter rotating beam of oppositely charged particles will generally "kill" any bunches apart from the targeted bunch due to the mismatch in particle number and their crossing at inappropriate sites in the rings. (Colliding-beam storage rings for high-energy physics are designed with great pains so that oppositely charged particle beams collide only when approximately equivalent in size and only at well defined positions around the storage ring.) hence, in accelerators operated specifically for colliding-beam high-energy physics, the temporal purity is generally very good.

It is important to recognize that the temporal characteristics of synchrotron radiation described above: pulse duration, interpulse period and temporal purity; are the same for all emitted wavelengths of radiation, i.e., the temporal properties are wavelength independent (Benard and Rousseau 1974, Lopez-Delgado 1978).

Table 1
X-ray storage rings

Facility	Stored beam energy (GeV)*	Critical photon energy (keV)*	Orbital period (ns)	Number of equally spaced *bunches*	Interpulse period (ns)	Bunch duration FWHM *(ps)*
ADONE Frascati, Italy	1.5	1.5	350	3 18	117 19.4	776
LURE (DCI) Orsay, France	1.7	3.1	316	1	316	1780
ADVANCED LIGHT SOURCE Berkeley, CA (under const.)	1.5 (2)	1.9 (4.4)	656	1 250	656 2.62	 25–50 6[d]
SRS Daresbury, UK	2.0	3.9	320	160	2	200
Photon factory Tsubuka, Japan	2.5	4.0	624	312	2	160
NSLS (X-ray) Brookhaven, NY	2.5	5.0	568	30	18.9	1700
SSRL (SPEAR) Stanford, CA	3 (4)	4.7 (11.1)	760	4 × 4[a] 4[b] 1[c]	187 × 2.8[a] 190 760	300
HASYLAB (DORIS) Hamburg, FRG	3.7 (5)	7.8 (22.9)	960	60 170 1[c]	16 8 960	200
VEPP-4 Novosibirsk, USSR	4.5 (5.8)	12.2 (26.1)	1220	1	1220	400
CHESS (CESR) Ithaca, NY	5 (8)	8.7 (35.5)	2560	1 3 7	2560 853 366	160

European Synchrotron Radiation Fac. (ESRF) Grenoble, France (under const.)	6	19.2 9.6	2816	1 992	2816 2.84	50
Advanced Photon Source Argonne, IL (under const.)	7	16	3536	1 20	3536 177	116
PEP Stanford, CA	15	45.4	7400	3	2467	70

*Parenthetical numbers indicate maximum design parameters.
[a]Four equally spaced groups of four adjacent bunches.
[b]SSRL periodically runs in a timing mode with four equally spaced bunches.
[c]Parasitic running conditions.
[d]Special low-current running.

2.4. Modifying the natural time structure of the source

No matter what the time structure is for a particular synchrotron-radiation source, it will not be optimal for all time-resolved experiments. While some experiments will require high repetition rates, others may need "long" periods of darkness preceding and/or succeeding a short burst of X-rays. (Long is used in this context as any time period greater than the interpulse period.) The natural time structure of a monochromatic X-ray beam can be altered through the use of modulating monochromators. Michael Hart, who considered this problem several years ago, has listed several possibilities including rotating and vibrating crystals (Hart 1980) and interferometric devices (Hart and Siddons 1978) capable of working at megahertz frequencies which can transmit one or several X-ray burst(s) to an experiment. Different approaches must be taken for white-beam modulation. One technique is to use fast kicker magnets (wobblers) that can deflect one (or several) particle bunch(es) out of the nominal orbit for a short distance and then return them to the unperturbed orbit. In this case, the experiment must be arranged so that it can see X-rays only from the deflected bunch(es). Wobblers such as these would allow the repetition rate of the X-rays impinging the sample to be varied from a single burst to rates determined by the duty cycle of the kicker magnets. A serious concern with wobblers is their effect on the emittance, stability and lifetime of the rest of the stored beam. A more passive approach to white-beam modulating, in the sense that it does not directly act on the stored beam, is through the passive use of choppers. Depending on the natural interpulse period, slotted chopper wheels can pass one (or several) bursts of X-rays while blocking preceding/succeeding bursts. For instance, a 0.5 mm aperture can be shuttered in 1.5 ms with a chopper wheel 30 cm in diameter rotating at about 21 000 RPM. A single-slotted chopper synchronized to the orbital frequency of the storage ring would pass a burst of X-rays every 2.8 ms. Higher rates could be attained by adding more slots, while lower rates could be achieved by using two chopper wheels or a chopper wheel and a mechanical shutter in series. Although rotational frequencies of 21 000 RPM may seem high, neutron or Fermi choppers routinely operate at these angular velocities and hence the required engineering technology already exists for the implementation of such devices. [See Mills (19??) for more information on the use of chopper wheels with X-rays.]

2.5. Comparison with other pulsed X-ray sources

It is constructive to compare the temporal properties of synchrotron radiation with other sources of pulsed X-rays in order to appreciate what advantages might be afforded in utilizing synchrotron radiation for investigation of transient phenomena. Such a comparison is displayed in table 2. Several points are immediately obvious. First, synchrotron sources have a truly continuous spectrum while most other sources have a mix of characteristic wavelengths and background Bremstrahlung radiation. Second, except for some laser generated sources, synchrotron radiation has the shortest pulse duration. And finally, there are currently no other sources of X-ray radiation that operate at megahertz repetition rates with the same power per burst one can obtain from radiation emitted by high-energy storage-ring sources. Although

Table 2
Pulsed X-ray sources.

Source of X-rays	Pulse length (ns)	Repetition rate (Hz)	Spectral properties
Pulsed X-ray generators	10–100	1–100	characteristic X-ray lines from anode (5–20 keV range) and some bremsstrahlung
Laser-produced plasmas	0.1–10 (same duration as laser pulse)	0.0001–0.01	bremsstrahlung and some discrete lines (0.5–5 keV range)
Pulsed electron linear accelerators	10–10.0	0.1–100	mostly bremsstrahlung (can be very hard)
Synchrotron-radiation sources	0.05–2	0.4–50	continuous spectrum (infrared–hard X-rays)

laser sources may equal or exceed the instantaneous flux from a single burst of synchrotron radiation, the high collimation of the beam from the storage-ring source facilitates directing those photons on to the sample and, therefore, the number of photons incident on a sample from a single laser shot or synchrotron burst may be comparable. The favorable comparison of synchrotron radiation with other sources of pulsed X-rays gives some indication of the marvelous potential for time-resolved studies that synchrotron radiation provides.

3. *Methodology of time-resolved experimentation*

All time-resolved experiments use some sort of pump/probe technique to investigate the time evolution of transient or short-lived states. The word pump is used here in the most general sense and can include such things as mixing, mechanical stressing, thermal excitation, photon excitation, electromagnetic excitation, etc. As the time-scales of interest decrease, the ability to excite the sample both rapidly and uniformly becomes increasingly critical. The time necessary to fully excite the sample can be, in some circumstances, the determining factor in the ultimate temporal resolution that is achievable. To increase the speed and uniformity with which the sample can be excited, larger pumps and/or smaller samples are used. The move towards smaller samples puts further demands on the brightness of the source and the focusing properties of X-ray optics.

Pump probe experiments can be divided into two categories:

(1) those experiments involving irreversible processes that must be studied on a one shot basis; and

(2) those experiments involving processes that can be cyclically pumped and hence signal averaged over many excitation periods. To date, experiments in the first class have successfully been performed using synchrotron-radiation sources with temporal resolutions in the millisecond regime; limited primarily by intensity considerations. On these timescales, the modulated time structure of the radiation is not explicitly used and the pump need not be synchronized to the arrival of the X-ray bursts. The resolution obtained in these experiments is generally determined by the amount of time required to collect statistically significant data. When the sample can be cyclically pumped or probed, standard signal-averaging techniques can be employed to build up the required statistics. If the lifetime of the excited state begins to approach the interpulse period on the X-rays, synchronization of pump pulses can be used to sample the evolving system at discrete times. For excitation-decay times less than the interpulse period, the relative time between the pump and X-ray bursts must be varied to allow the entire lifetime of the transient state to be explored. One of the most efficient time-resolved techniques is realized if the system can be pumped or excited at (or at a multiple of) the X-ray repetition frequency so that each burst of X-rays is used to sample the transient state. Stroboscopic methods are also attractive in that nanosecond (or better) temporal resolution can be obtained with integrating detectors, such as film. A summary of some pump and detector speeds along with representative timescales of a variety of physical phenomena is shown in table 3.

In the discussions above it has been tacitly assumed that the X-ray beam will be used as the probe beam and the pump will be supplied by some external apparatus. This, of course, need not be the case as the X-ray pulse itself can be used as the exciting beam. For certain classes of experiments that use the X-rays as a pump, phase-shift methods (Gratten and Lopez-Delgado 1979, Rehn 1980) may prove useful. Phase-shift methods are ideally suited to the natural time structure of the synchrotron radiation and could have temporal-resolution capabilities of a hundredth of the bunch duration, making picosecond and perhaps subpicosecond measurements feasible.

The particular characteristic of the radiation that is most important can be a function of the timescales involved. For experiments with temporal resolutions of milliseconds, the pulsed nature is not used and average intensity is critical. Experiments that do use the modulated time structure may rely more heavily on the instantaneous intensity or simply on the number of photons per burst. Instantaneous intensity is dependent upon the average intensity of the number of bunches in the storage ring and the bunch duration. The source with the highest average intensity may not necessarily have the largest instantaneous intensity or maximum number of photons per burst.

The physical foundations for the basic X-ray techniques (small-angle scattering, diffraction, topography, absorption spectroscopy, etc.) used in time-resolved experiments are often the same as those in static measurements. Since these topics have been dealt with in detail in this and other books, discussions here will be limited to those of

Table 3

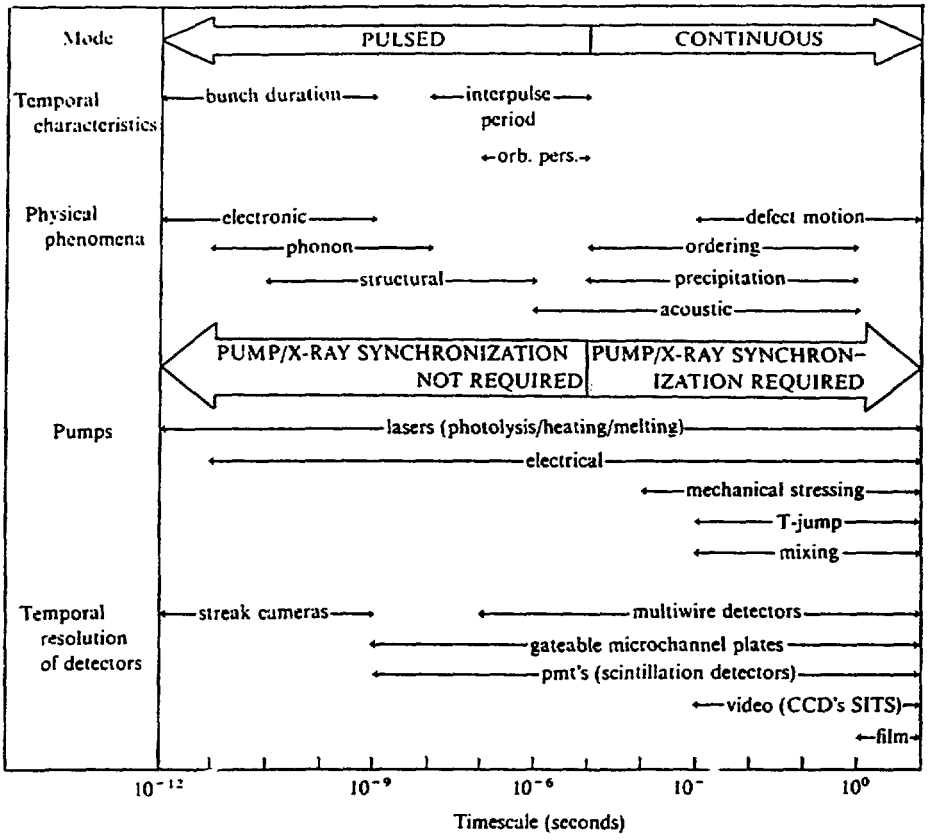

experimental methods that are particularly unique to the temporal-resolving aspects of the experiment. In many circumstances, extending a measurement from the static to the time-resolved regime requires only the replacement of a slow or integrating detector with a fast (and sometimes gateable) detector. In other instances, entirely new techniques have been developed to facilitate temporally resolved studies as in the case of energy dispersive X-ray absorption methods. Although there is often much overlap, three major divisions of time-resolved experimental techniques can be constructed. These are experiments that

(1) are intensity dependent;
(2) depend upon the continuous spectral nature; and
(3) rely on the modulated temporal structure of the emitted radiation.

3.1. Intensity dependent experiments

Although firm boundaries between various techniques are difficult to draw, the experiments and experimental techniques described under this heading all rely

principally on the increased flux available at synchrotron sources over what would be generally available from conventional laboratory sources.

The potential application of the increased flux available from synchrotron-radiation sources to performing time-resolved scattering experiments was recognized in the 1970s. Several of these pioneering experiments, including the beautiful work of Huxley et al. on the investigation of the kinetics of muscles (Huxley et al. 1982) were performed at the European Molecular Biology Laboratory's (EMBL) outstation in Hamburg; one of whose major thrusts was to develop techniques for the study of dynamic phenomena in biological systems (Bordas et al. 1980). These initial time-resolved X-ray small-angle scattering (SAXS) experiments were performed with a one-dimensional gas proportional counter with a delay-line readout (spatial resolution 400 μm and maximum count rate 5×10^5 counts/s). In experiments such as this, single-wire detectors are most often the limiting element in the improvement of temporal resolution. By replacing single-wire counters with multiple-wire counters, each having its own amplifier and associated electronics, count-rate capabilities can be greatly expanded. With several hundred wires, e.g., detector count-rate capabilities in the 100 MHz regime can be attained allowing for much shorter time-slices.

Time-resolved SAXS experiments using one-dimensional detectors (wire, CCD, diode arrays) have been used for the investigation of muscle contractions (Huxley et al. 1982, Bordas et al. 1980, Wakabayashi et al. 1985, Wakabayashi et al. 1986) phase transitions in lipids (Letellier et al. 1981, Ranck and Mouden 1979), polymerization of tubulin (Mandelkow et al. 1980), structural changes during reversion in alloys (Osamura et al. 1985), and the kinetics of phase separation and ordering in binary alloys (Stephenson 1988, Sutton et al. 1988).

When two-dimensional detectors are required, it has been the general trend to move from wire counters to video systems, because of the inherent low count-rate capabilities of the conventional multiwire detectors and the rapidly increasing cost and complexity of multiple amplifier systems. Video systems can come in a variety of arrangements, depending on how the X-ray image is converted into a video signal. [For an excellent review on two-dimensional video detectors, see Gruner et al. (1982).] X-ray-to-video signal conversion can be done directly by using an X-ray sensitive camera (Tuomi et al. 1980, Chikawa and Fujimoto 1968) or by down converting the X-rays into visible photons (usually via some fluorescent material) which are then recorded by a standard video camera (Hartmann 1980, Bowen et al. 1982). (When using a fluorescent screen for photon down conversion, it is important that the fluorescence lifetime of the converter is shorter than the dynamic process that is to be observed.) In many situations, the visible photons need to be amplified before being viewed by the video camera. This can be accomplished by means of image intensifiers or microchannel plates.

Video systems usually have somewhat small active areas, typically 1–10 cm^2, but in general are quite adequate for most topographic or SAXS applications. Depending on the field of view, spatial resolutions of better than 10 μm can be obtained (Tanner et al. 1983). Care must also be exercised in order that geometrical distortions, such as pin-cushioning, are kept at a minimum and that intensity levels are kept in a range where bloom or pixel overflow is minimized. Video cassette recorders are used to record the

data for off-line analysis. The standard framing format for video systems in the United States is 30 Hz (corresponding to a temporal resolution of 33 ms per frame) and 525 lines per frame. High-speed video cameras are available with framing rates of over 1000 Hz, allowing one to push the temporal resolution of the detector to less than a millisecond. Except for the most strongly scattering samples, kilohertz exposure rates are generally not obtainable.

A considerable number of small-angle X-ray scattering investigations have utilized such detectors. (The reader is referred to chapter 11 for details of SAXS.) A typical setup for SAXS with a two-dimensional video recorder is shown in fig. 4. Areas of active research include phase transitions of lipids (Caffery et al. 1983, Caffery 1985, Caffery 1987), polymers (Prieske et al. 1983), craze formation in polymers during stress cycling (Grubb and Liu 1984), assembly processes in viruses (Berthet-Colominas et al. 1984), and enzyme dissociation (Fowler et al. 1983).

Time-resolved X-ray topographic studies rely on video systems similar to those described for small-angle X-ray scattering for real-time imaging. (For a fuller discussion on topographic techniques see chapter 10.) Temporal resolution is again determined by the framing rate of the video system (usually 25–30 Hz). Real-time topographic studies can be made with either a monochromatic beam or using the full white beam. Areas of research utilizing real-time topographic studies include magnetic

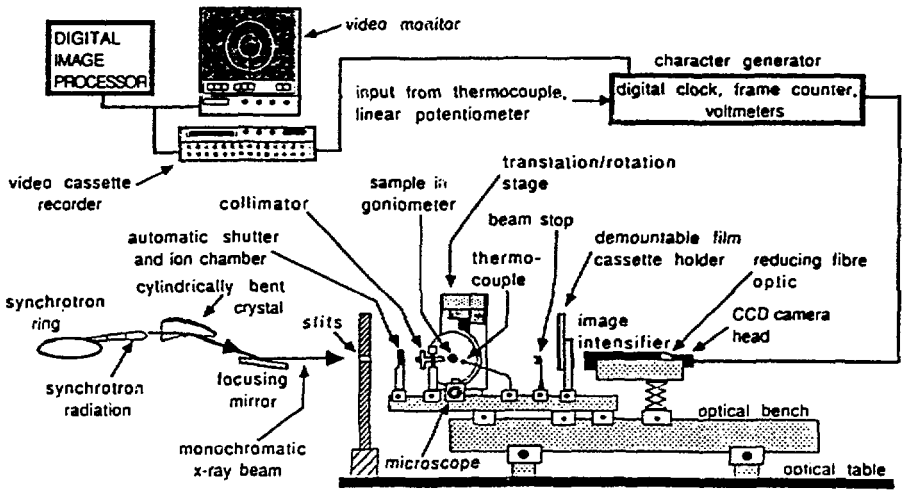

SCHEMATIC OF THE TIME-RESOLVED X-RAY DIFFRACTION SYSTEM

Fig. 4. Schematic representation of a time-resolved small-angle scattering set-up. Synchrotron radiation is monochromated and focused before entering the experimental station. After going through slits and collimators, it strikes the sample. The scattered radiation is detected by an X-ray image intensifier and the intensified diffraction pattern is recorded by a video camera. The diffraction pattern is stored on a video cassette recorder. By using a character inserter, experimental parameters (temperature, pressure, pH, etc.) can be written onto each frame so that the scattering data is synchronized to any external perturbation (figure courtesy of M. Caffery).

domain motion under the influence of external magnetic fields in Ni (Boettinger et al. 1982), Fe whiskers (Chikoura and Tanner 1978), rare-earth–Fe alloys (Clark et al. 1979), and Fe–3.5%Si (Miltat and Kleman 1979), recrystallization kinetics in Fe–3.5%Si (MacCormack and Tanner 1978), Al (Gastaldi and Jourdan 1978), Ti (Jourdan and Gastaldi 1983), grain-boundary motion (Gastaldi and Jourdan 1984), phase transformations (Ribet et al. 1985), dislocation motion (Suzuki et al. 1984), and bending and stress (Toumi et al. 1983, Miltat 1978) studies.

Wide-angle X-ray scattering experiments with temporal resolutions ranging from several seconds to several milliseconds generally use standard detector arrangements and simply route the diffraction data into several different counters or channels at predetermined times after the pump. Hence, each channel represents a different time slice. If the shape of one diffraction peak (or several peaks that are in close spatial proximity) is to be monitored as a function of time, one- or two-dimensional detectors can be employed. Depending on the type of detector, the data-collection rate or the readout time may determine the ultimate temporal-resolution rate achievable. One shot or irreversible processes have been recorded in less than one second. However, to push the timescales down further, signal averaging over many cycles is required. Bartunik (1983) and co-workers have investigated the crystalline MbCO following laser flash photolysis in such a manner, with a temporal resolution of $\simeq \frac{1}{2}$ ms (fig. 5).

Tamagai et al. (1984, 1985) have studied the electric-field induced deformation in sliding charge-density waves (CDW) in $K_{0.30}MoO_3$ with wide-angle X-ray scattering.

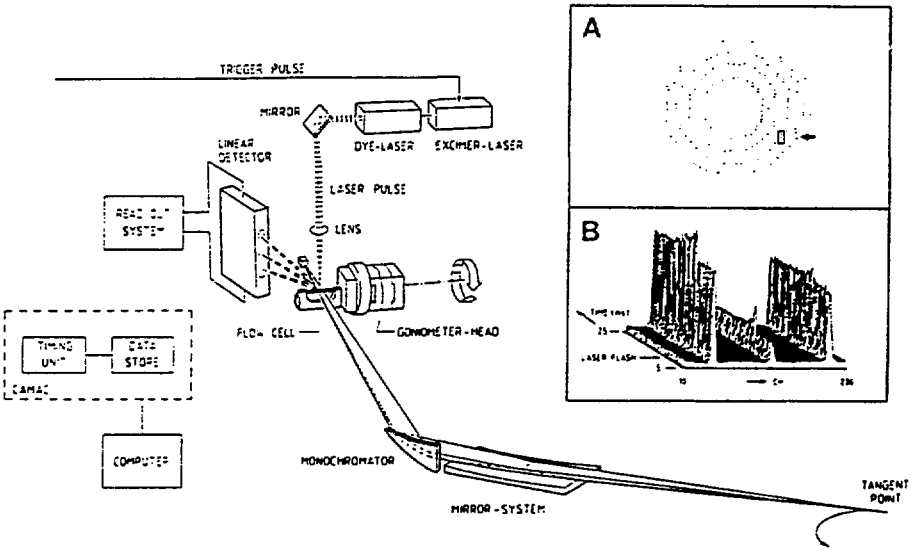

Fig. 5. Schematic set-up of time-resolved X-ray diffraction from crystalline MbCO. From a portion of the total diffraction pattern (*a*), three diffraction spots (boxed) are chosen to be monitored by a linear position sensitive detector (PSD). The output of the PSD versus time (*b*) shows the changes in the diffracted beam intensities following sample excitation via a pulsed dye laser (Bartunik 1983).

In their work, a periodic current pulse was applied to a single crystal of the material and the evolution of both the intensities and positions of satellite reflections were monitored with a temporal resolution of 200 μs.

As can be inferred from the list of different materials that have been studied using time-resolved X-ray scattering and topography, a variety of techniques of specimen perturbation/pumping have been developed. Stopped-flow, pH-jump and temperature-jump (*T*-jump) techniques, mechanical stressing, electrical stimulation, and photon excitation have all been used in conjunction with time-resolved X-ray measurements. A *T*-jump device has been described by Renner et al. (1983) having four water baths at −20, 0, 37, and 70°C (fig. 6). With this arrangement, temperature jumps from 0 to 37°C and the reverse were obtained by bathing the sample briefly with the solution at the higher temperature followed by a bath with a solution at the desired temperature. In this fashion, temperature changes of 37°C could be made in several seconds. Investigation of polymerization in microtubule proteins using *T*-jump techniques such as those described above have been made with a temporal resolution of tens of seconds.

Several groups have developed stopped-flow cells for time-resolved scattering (Berthet-Colominas et al. 1984, Fowler et al. 1983) and spectroscopy (Nagamura et al. 19??, Matsushita et al. 1984a) studies. Stopped-flow techniques are among the most convenient way of investigating the kinetics of solutions in the time range of seconds down to milliseconds. Stopped-flow cells consist of two (or more) pistons that can inject solutions usually into a *T*-mixer and finally into the sample cell as shown in fig. 7. (If signal averaging is required an additional reservoir is included to flush the system between mixings.) The sample cell must have relatively thin X-ray windows (typically mica or Be) and caution must be exercised since these can flex causing variations in sample thickness due to the pressure from the injected solution. Mixing times on the order of 20–100 ms can be obtained depending on the size of the cell.

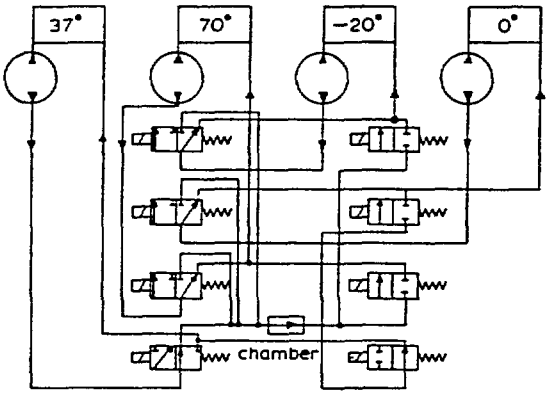

Fig. 6. Block diagram of a four-reservoir bath for temperature-jump experiments. Rapid temperature changes from 0 to 37°C and the reverse are made possible by exposing the sample chamber to brief overshoots of colder (−20°C) or warmer (70°C) baths before the baths of the desired temperature are applied (Renner et al. 1983).

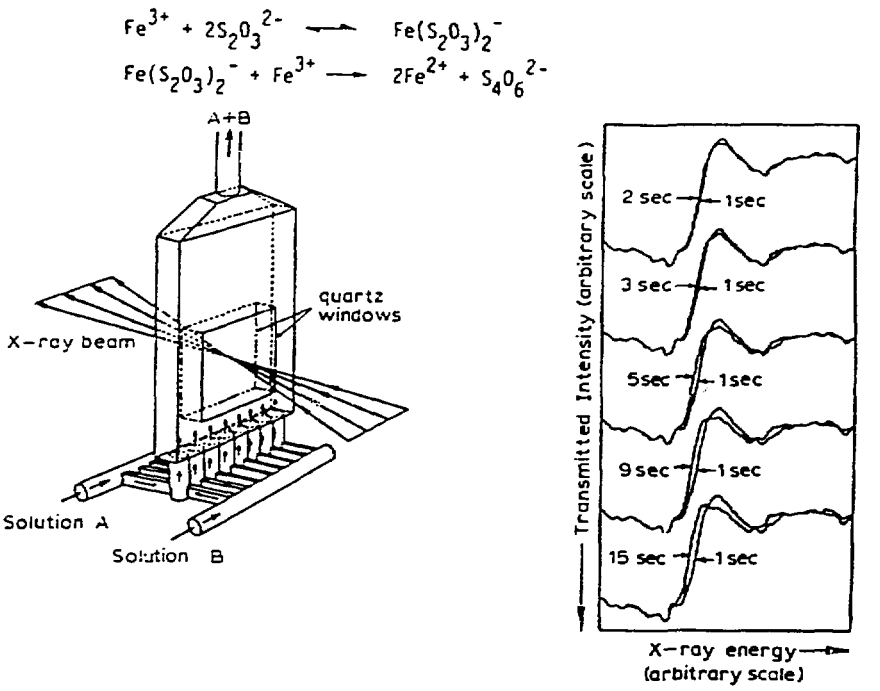

Fig. 7. Schematic diagram of a stopped-flow cell constructed for time-resolved dispersive EXAFS measurements. In this cell design, the mixed solution ($A + B$) reaches the volume illuminated by the X-rays in about 6 ms. A temporal resolution of about 1 s was obtained with this set up (see spectra on right) (Matushita et al. 1984a, b).

To bridge the temporal gap between stopped-flow techniques and relaxation methods (see following section), continuous- or regenerative-flow devices (fig. 8) can often be used with X-rays. In a continuous-flow system, the reactants are initially mixed and are forced (usually via a piston/syringe device under gas control) to flow past a view point at which the X-ray measurement is made. The farther away from the mixing point the observation is made, the later the reaction is viewed in its time-course. With flow velocities in the 10–50 m/s range, and a 1 mm high viewing slit, temporal resolutions of 20 μs, with absolute time errors of $\simeq 50$ μs can be obtained (Chance et al. 1967). Chance and co-workers (Chance et al. 1984, Chance 1984) have also used continuous-flow techniques in conjunction with X-ray absorption spectroscopy. In their apparatus (with which they wish to study the structure of horseradish peroxidase–peroxide compounds), the temporal design parameters were: time resolution in the millisecond range; observation time before remixing of $\simeq \frac{1}{2}$ s; and mixing repetition frequency of 1 s. Up to 80 mixings could be performed before data recording was discontinued in order to refill the appropriate reservoirs with reactants, and the experiment restarted.

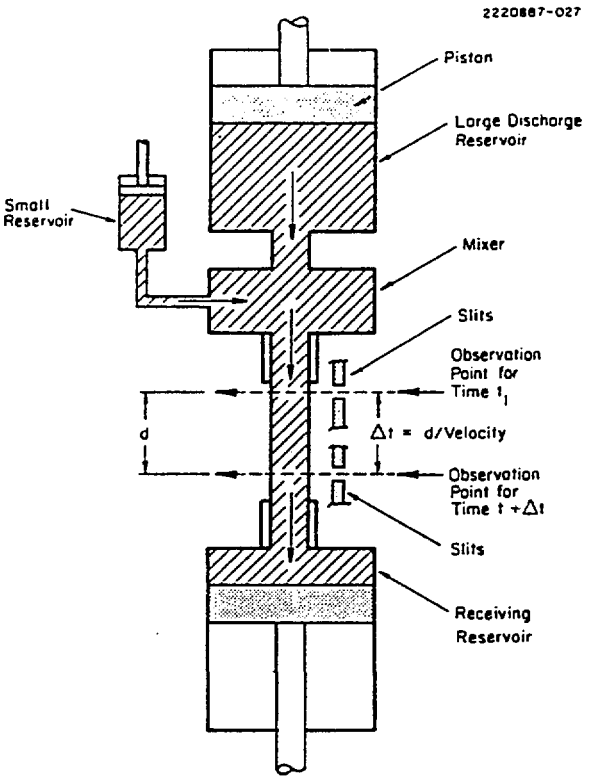

Fig. 8. Schematic diagram of a continuous-flow cell. The two reactants are held in separate reservoirs until the mixing sequence is initiated. Pistons force the reactants into the mixing volume and then past the viewing window into the receiving reservoir. The greater the distance between the observation point and the mixer, the further along in the time course of the reaction one observes. The observation point can easily be determined by a set of slits.

3.2. Continuous-spectrum experiments

Not all time-resolved experiments are currently limited by detector or electronic considerations; some are simply X-ray flux limited. Given that presently operating synchrotron-radiation sources will only be able to increase their flux output by approximately an order of magnitude with new insertion devices, other solutions must be sought for those time-resolved experiments that are truely photon limited. One approach to this problem is to increase the bandpass of the radiation incident on the sample. For many experiments, this is quite an acceptable solution. Perfect single-crystal monochromators have a high reflectivity over a very narrow energy range, typically several electron volts at X-ray energies corresponding to a bandpass of 10^{-3}–10^{-4}. For those experiments that can tolerate larger energy spreads, factors of 10–100 in the incident flux may be realizable (with commensurate decreases in

exposure times) by using wide-bandpass optical components. Wide-bandpass X-ray optical devices have been under investigation by many groups. Two approaches look most promising: strained or graded d-spacing perfect crystals and layered synthetic microstructures (LSMs). With strained or graded d-spacing crystals, a polychromatic beam of X-rays is allowed to strike the crystal at some fixed angle. A given X-ray photon penetrates the crystal until it "finds" the lattice spacing that satisfies the Bragg law for its wavelength and is then scattered out. Fukuhara and Takano (1980) have looked at this from both an experimental and theoretical point of view. By growing a boron-doped epitaxial layer on a single silicon crystal, they have increased the X-ray integrated intensity of this crystal by a factor of four. Theoretical studies of reflection curves for silicon have also been made. When a linear strain gradient of $-1 \times 10^{-3}/28$ μm (introduced via impurity diffusion) was considered, regions of high reflection with widths over 100 arcsec were predicted with a corresponding increase in the integrated intensity by almost an order of magnitude at 7 keV. But even with this increased reflectivity width, the bandpass of the crystal would be much less than 1%. Mosaic or imperfect crystals offer wider angular acceptances; unfortunately, the mosaicity is generally so large (typically tenth of a degree or more) that it destroys the natural collimation of the synchrotron beam and so intensity increases (flux/unit area) are not large.

One promising new X-ray optical element is the layered synthetic microstructure or LSM. These artifically produced structures consist of alternating layers of high and low atomic-number materials. In general for a LSM of N layers, the energy resolution should scale as $1/N$. Bilderback et al. (1983) have characterized several LSMs (fig. 9) and shown that bandpasses in the several percent regime are readily achievable with high reflectivities ($\simeq 70\%$). Work is now being carried on by several groups to explore the possibility of producing focusing multilayer optical systems which could produce gains of several orders of magnitude in intensity over flat perfect-crystal X-ray optical systems. Such systems would be ideal for many time-resolved applications, in particular small-angle X-ray scattering studies.

As a first step towards this goal, Stephenson and colleagues have developed a monochromating system for small-angle X-ray scattering comprising a bent cylindrical mirror and a pair of flat W–Si multilayers. This configuration provides an intensity of 10^{13} photon/s mm^2 at 6 keV in $\simeq 1\%$ bandpass (Stephenson 1988) at the National Synchrotron Light Source (NSLS). With this monochromating system, in conjunction with a linear photodiode array, kinetic studies of crystallization, phase separation and ordering phenomena have been made (Stephenson 1988, Sutton et al. 1988), some with a time-resolution of 3 ms.

X-ray optical systems with even larger bandpasses have been considered for use with time-resolved protein crystallography. These typically consist of a filter/external-reflection mirror combination; the filter provides the low-energy cut-off and the mirror provides the high-energy cut-off. Two mirror systems, with one mirror operating in a transmission mode, have also been considered (Lairson and Bilderback 1982), but difficulties in producing a stable transmission mirror have limited the usefulness of this method. Using such a wide-bandpass optical system (or the white beam directly) and taking advantage of the continuous nature of the spectrum emitted

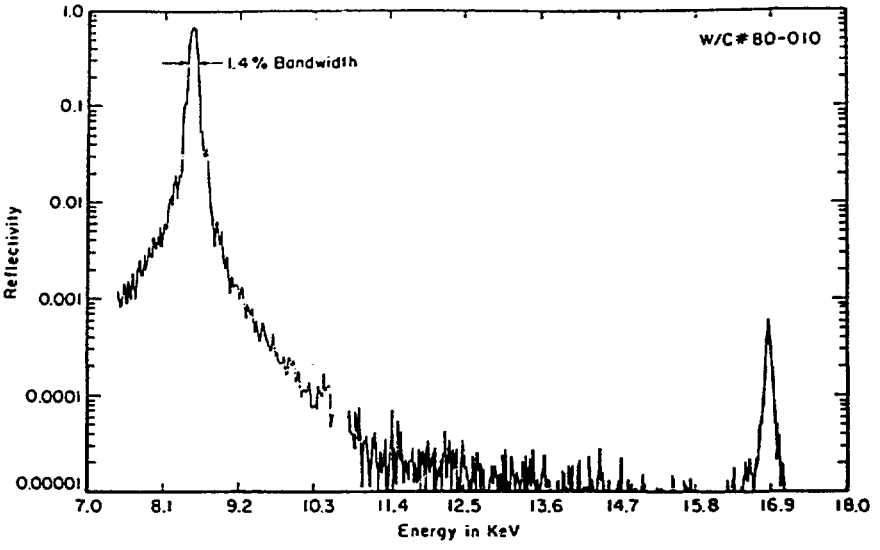

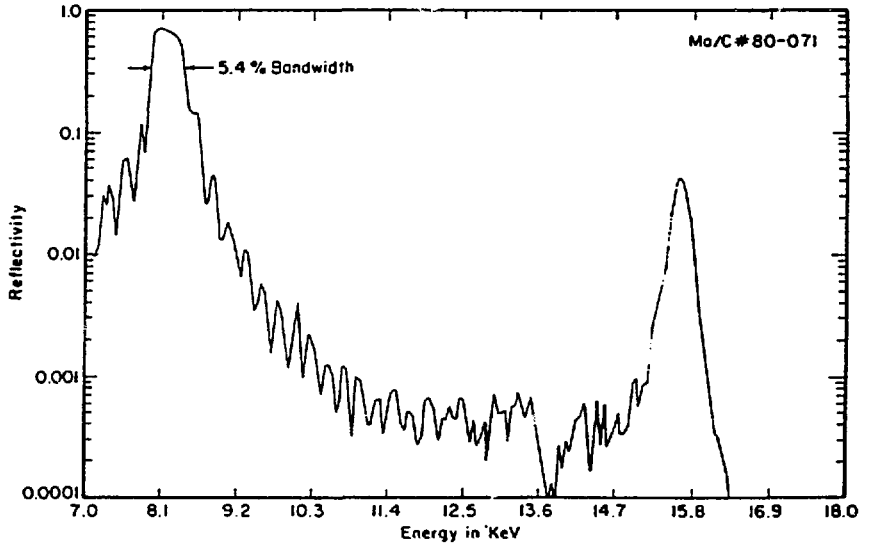

Fig. 9. Reflectivity as a function of energy for two layered synthetic microstructures (LSMs). (a) A 100-layer tungsten-carbon LSM ($d_W = 8.56$ Å, $d_C = 12.84$ Å, $d = 21.4$ Å) shows a reflectivity of 66% at the fundamental with a $\Delta E/E$ of 1.4%. (b) By decreasing the number of layers to 30 ($d_W = 26$ Å, $d_C = 30$ Å, $d = 56$ Å), the bandpass can be increased to 5.4% with over 70% reflectivity in the fundamental (Bilderback et al. 1983).

from synchrotron-radiation sources, parallel data-collection schemes can be employed where data are collected at a variety of wavelengths simultaneously. One application of this technique is time-resolved crystallography. Utilizing Laue diffraction geometries with polychromatic radiation incident on a stationary sample (rather than using a monochromatic incident beam and rotating the sample to obtain an integrated intensity as in conventional oscillation or procession photography), the integrated intensity is obtained through wavelength integration rather than angle integration (Helliwell 1986, Moffat et al. 1984). With the Laue geometry, a large number of reflections can be recorded simultaneously with a two-dimensional detector (most commonly X-ray sensitive photographic film), thereby permitting a marked reduction in data-collection time over that of a rotating-crystal arrangement. Even with the presently available wiggler sources and focusing optical systems, conventional monochromatic-beam protein crystallography exposures of several 10's or 100's of seconds are required. Using wavelength-integration techniques, photos of comparable quality have been obtained for hemoglobin-protein crystals with exposures under one second. Exposure times in the millisecond regime have already been shown to be feasible.

The principles of this technique can be illustrated by using the Ewald construction method as shown in fig. 10. If a well-collimated polychromatic beam of radiation with wavelength spread $\Delta\lambda = \lambda_1 - \lambda_2$ strikes a crystal, the Bragg condition for diffraction will be satisfied by all the reciprocal-lattice points that lie between the two limiting spheres of reflection; having radii $1/\lambda_1$ and $1/\lambda_2$. A primary concern of this technique is that of multiple Laue reflections, i.e., two or more reflections having the same 2θ values and, therefore, striking the film at the same location. Overlapping reflections complicate the problem of extracting the individual structure factors. If the wavelength spread $\Delta\lambda/\lambda$ is judiciously selected, this problem can be minimized. The condition for a Laue spot on the film to be from a single reflection (i.e., due to one structure factor) is that $m\lambda \leqslant (\lambda_1\lambda_2)/\Delta\lambda$, where m is the order of the reflection and λ is the wavelength satisfying the Bragg law for reflection (*mh*, *mk*, *ml*). Moffat et al. (1984) point out that for $\Delta\lambda/\lambda \simeq 0.2$, all reflections for which $m < 5$ will be from a single structure factor and hence multiple-order reflections are not a major problem. Several exposures using this technique are shown in fig. 11. Table 4 shows the decreases in exposure times that might be expected by using polychromatic techniques for protein crystallography studies. Because of the use of an integrating detector (i.e., films), the techniques described above have been used with one-shot type experiments. A gateable detector would allow for time-slicing methods, and dramatically decrease the temporal resolution if the sample could be cyclically excited, and radiation damage of the crystal did not pose a serious problem.

Experiments where intensity versus X-ray energy measurements are sought quite naturally lend themselves to parallel data-collection techniques. Two methods are particularly amenable to this concept: energy dispersive scattering (EDS), and energy dispersive extended X-ray absorption fine structure (EXAFS).

Time-resolved energy dispersive scattering has to date been used only for studying phase transformations. In a time-resolved EDS experiment a polychromatic synchrotron beam strikes the sample producing scattered radiation which is energy

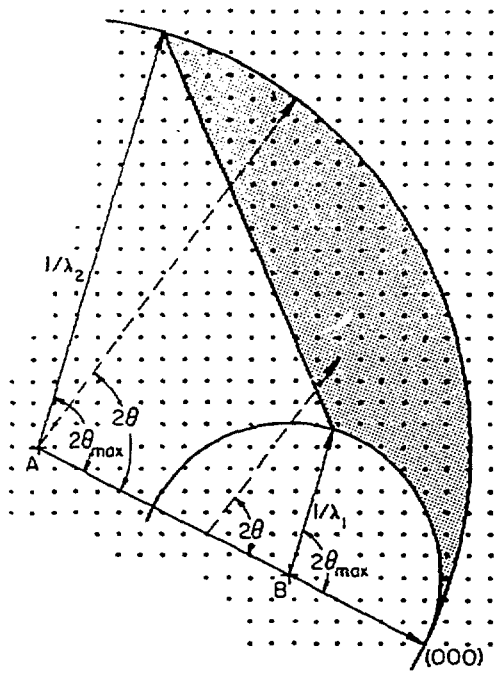

Fig. 10. Ewald construction of white-beam Laue diffraction technique. If the incident beam has a wavelength spread $\Delta\lambda = \lambda_1 - \lambda_2$, in principle all reciprocal-lattice points bounded by the two limiting spheres of radii $1/\lambda_1$ and $1/\lambda_2$ will be excited. In practice, there will be some maximum 2θ value which will limit the total number of excited points shown here as the shaded region. Reflections from two (or more) individual reciprocal-lattice points will overlap on the recording medium when they have equal 2θ values, as indicated by the two dashed lines in the figure.

analysed at a fixed scattering angle (fig. 12). The output from the energy dispersing detector, usually a Ge or Si solid-state detector (SSD) is then fed into a multi-channel analyser (MCA) for pulse-height analysis with a typical output shown in fig. 12. By monitoring the location and shape of the diffraction peaks as a function of time, the kinetics of phase transitions can be followed. In principle, it is desirable to monitor all the diffraction peaks. This is not possible in practice since SSD/MCA systems have maximum count rates of only several tens of thousands of counts per second. Therefore, in order to decrease the data-collection time, only a limited number of peaks are monitored (Ayers et al. 1985, Hinze et al. 1983). This is a classic situation where detection technology is the limiting factor in decreasing the temporal resolution.

Energy dispersive EXAFS is an exciting new spectroscopic technique where, rather than recording the absorption of the samples as a function of energy in sequential energy steps, a polychromatic beam is focused onto the absorbing sample. The transmitted diverging beam is then recorded with a linear detector. Because there is a

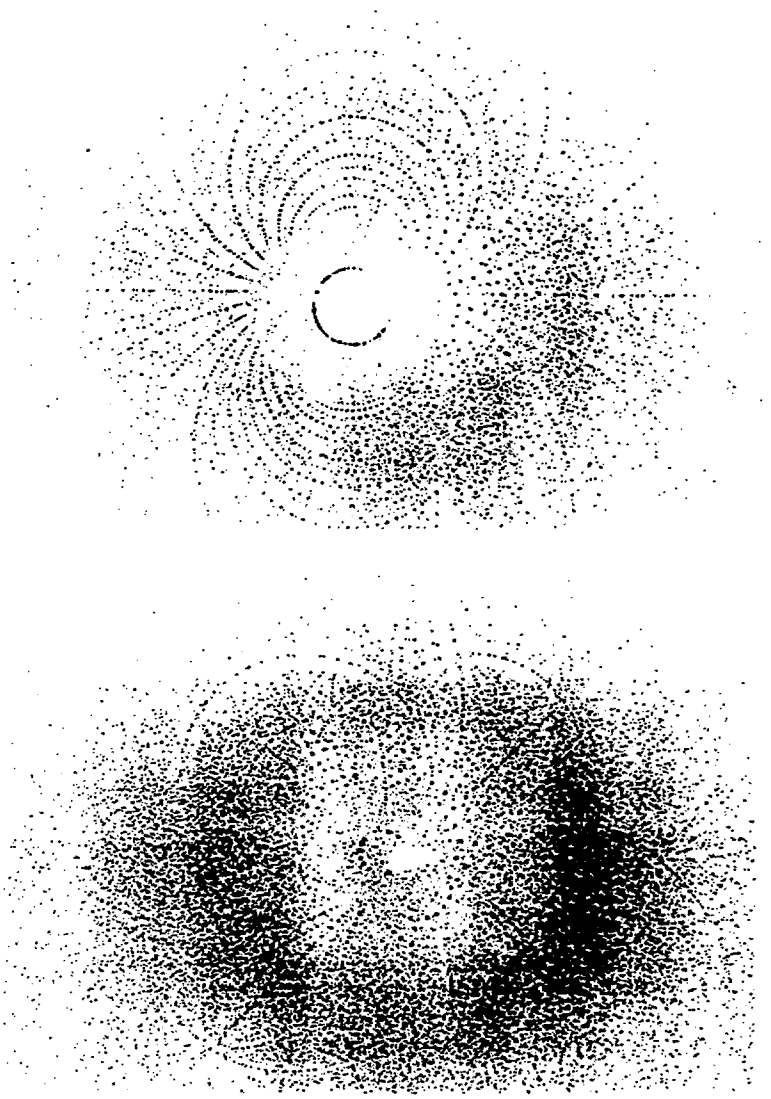

Fig. 11. Time-resolved Laue diffraction pattern of hen-egg white lysozyme taken at CHESS. Total external reflection from Pt-coated glass mirror set at 5.8 mrad plus 0.005 in Al foil yielded an X-ray beam with a wavelength range from 1.9 to 0.5 Å. Exposure time for these patterns, recorded on Kodak storage phospher plates, was 100 ms (courtesy of K. Moffat).

correlation between position and X-ray energy in the transmitted beam, measurements of intensity versus displacement can be translated into absorption versus energy curves.

The experimental geometry for energy dispersive EXAFS is shown in fig. 13. An elastically bent crystal (typically, a perfect Si or Ge crystal) acts as the dispersing

Table 4
Decrease in exposure times, expected by using polychromatic techniques

Source	Approximate intensity* (photons/s)	Minimum exposure (s)	Typical exposure (s)
Sealed tube X-ray generator, CuKα	5.0×10^6	500	20 000
Rotating-anode X-ray generator, CuKα, 6KVA	1.0×10^7	250	10 000
Synchrotron + wiggler + focussing crystal monochromator	2.5×10^9	1.0	30
Synchrotron + bend magnet + polychromator	2.5×10^{10}	0.1	1.0
Synchrotron + wiggler + focussing polychromator	2.5×10^{12}	0.001	0.01

*Through a 0.2 mm diameter collimator.

element, and focuses the polychromatic X-ray beam onto the sample. The diverging, transmitted beam then is recorded by a one-dimensional X-ray detector. Initially, the detector medium was film, but, more recently, solid-state devices have been employed. The energy spread, δE, incident on the sample (for a fixed source-to-crystal distance), is a function of the radius of curvature of the bent crystal, R, the length of the crystal, L, and the lattice spacing of the dispersing crystal and is given by

$$\delta E = E_0 L\left(\frac{1}{R} - \frac{\sin\theta_B}{P}\right)\cot\theta_B,$$

where P is the source-to-crystal distance and θ_B and E_0 the Bragg angle and energy of the central ray, respectively. With reasonably sized Si(111) crystals ($L \simeq 100$ mm), energy spread from 500 to 1000 eV can be achieved in the 5–10 keV range.

There are three contributions to the energy resolution of this arrangement (Matsushita and Phizackerly 1981), the finite source size, the spatial resolution of the linear detector and the intrinsic reflection width of the dispersing crystal (fig. 14). Following Matsushita and Phizackerly (1981), various contributions to the resolution for a symmetrically cut crystal can be written as follows. The energy spread due to the finite source size is given by

$$\Delta E_1 = \Delta S E_0 \alpha\left(\frac{1}{R\sin\theta_B} - \frac{1}{\alpha}\right)\frac{\cot\theta_B}{P-\alpha},$$

where ΔS is the width of the source and α a parameter (Moffat et al. 1984) given by

$$\alpha = \left[\frac{1}{\sin\theta_B} - \frac{1}{f_1 + f_2}\right]^{-1}.$$

where f_1 is the focus-to-detector distance, and f_2 the crystal-to-focus distance.

Laue deep

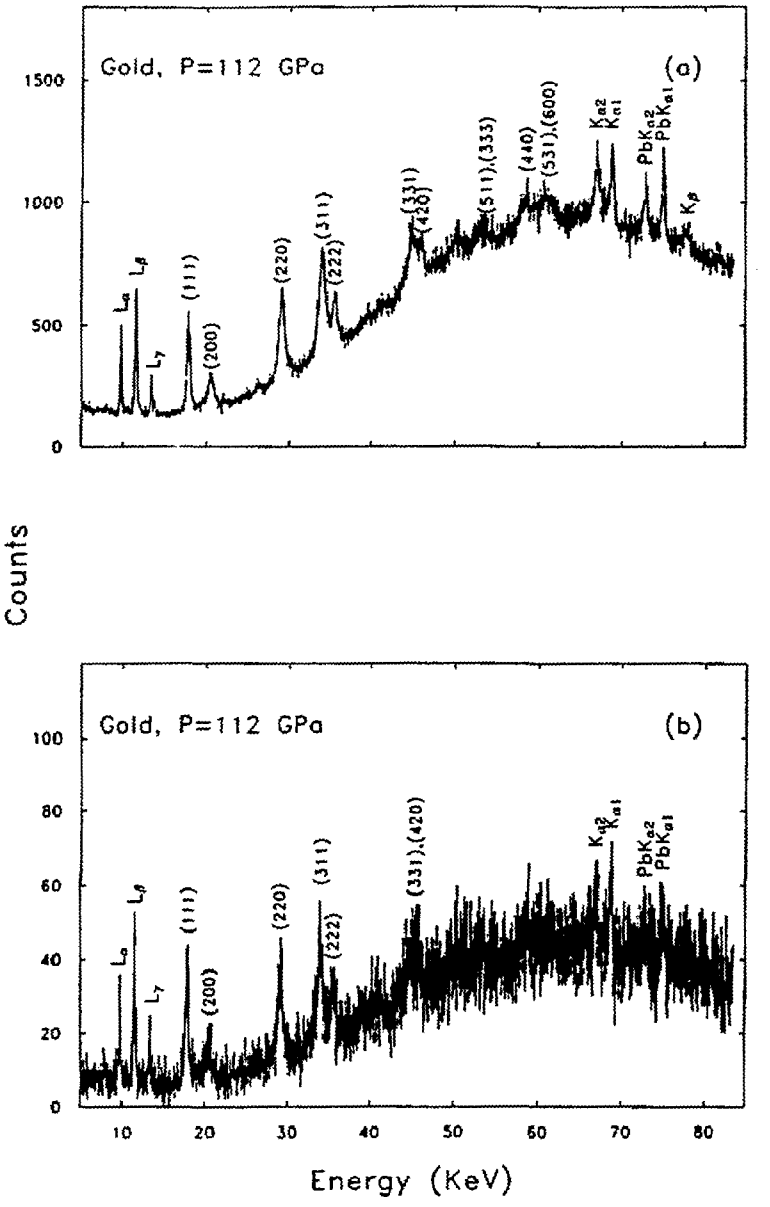

Fig. 12. Energy dispersive X-ray diffraction data. In (a) is the diffraction pattern for gold taken at a pressure of 112 GPa with X-rays emitted from the CHESS 6-pole wiggler collected in 5 min. In (b) is a gold pattern at the same pressure collected in 10 s in which 5 to 6 peaks are clearly identifiable. In (c) the experimental setup used to collect this data is shown. For more rapid time-resolved studies it may be necessary to monitor only one (or several) peak(s) because of detector and electronics count-rate limitations (courtesy of Z. Rudoff).

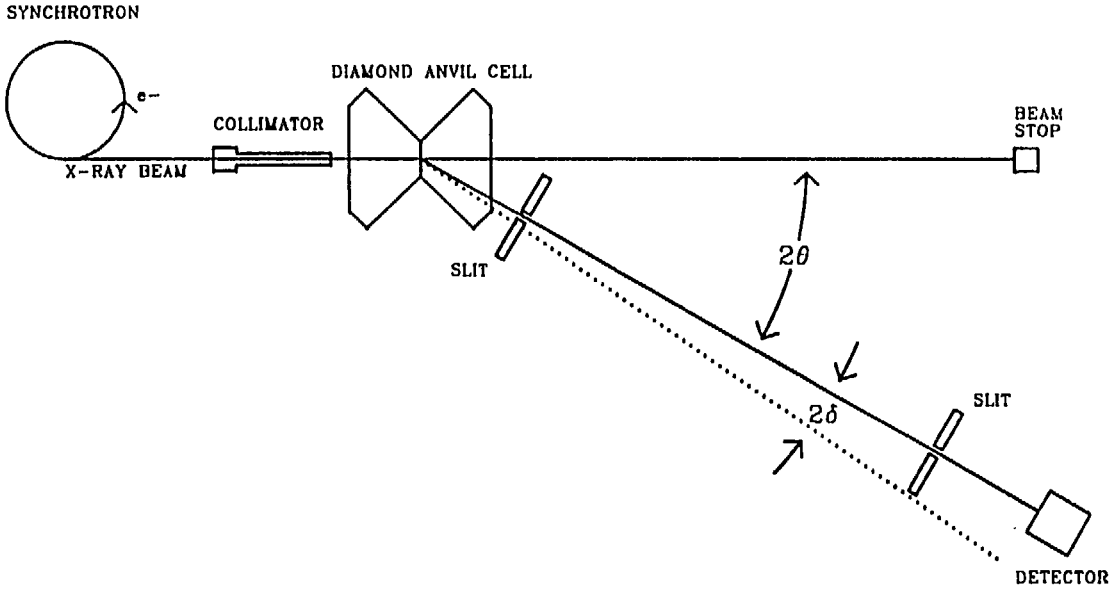
Schematic of Set-up
SYNCHROTRON
e-
X-RAY BEAM
COLLIMATOR
DIAMOND ANVIL CELL
SLIT
BEAM STOP
2θ
SLIT
2δ
DETECTOR

FIGURE 12(c)

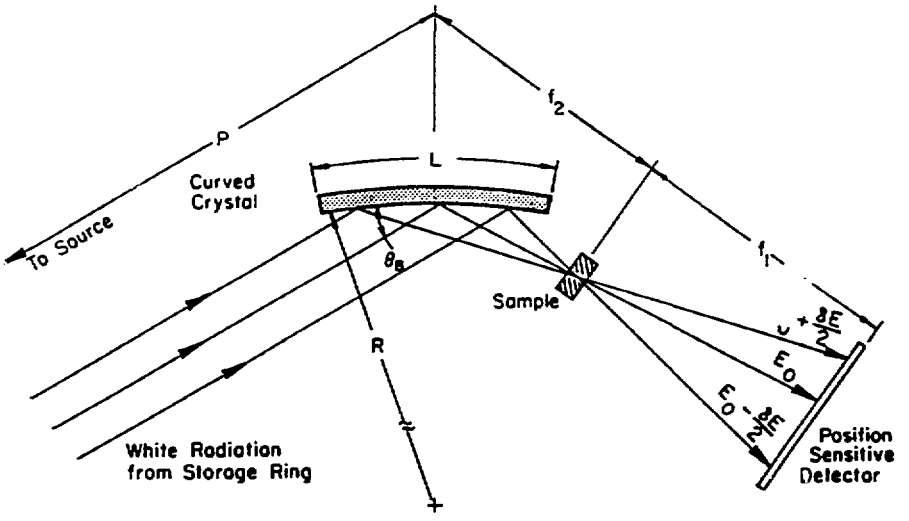

Fig. 13. Schematic representation of the experimental layout for dispersive X-ray spectroscopy. Synchrotron radiation is monochromated and horizontally focused by a curved, perfect-crystal monochromator. Because each ray across the face of the crystal impinges at a slightly different Bragg angle, there is a relationship between position and energy in the monochromated beam. By using a linear position-sensitive detector, all energies of an X-ray absorption spectrum can be recorded simultaneously.

The energy spread, ΔE_2, due to the detectors spatial resolution ΔX is given by

$$\Delta E_2 = E_0 \frac{\Delta X}{f_1} \left(\frac{\frac{P}{R} - \sin\theta_B}{\frac{2P}{R} - \sin\theta_B} \right) \cot\theta_B.$$

The energy spread due to the Darwin width, ω, of the crystal can be written as

$$\Delta E_3 = E_0 \omega \cot\theta_B.$$

Since these separate energy contributions are uncorrelated, the total energy resolution of the system is

$$\Delta E = [(\Delta E_1)^2 + (\Delta E_2)^2 + (\Delta E_3)^2]^{1/2}.$$

Matsushita and Philzackerly working at SSRL ($P = 17.5$ m, $f_2 = 0.3$ m, $R = 2.95$ m, $L = 100$ mm, $E_0 = 9.4$ keV) and using film ($\Delta X \simeq 25$ μm) have shown that a resolution of below 2 eV is possible with such an arrangement. If the temporal evolution of a system is desired, the film must be replaced by a linear detector capable of fast readout and high photon flux. One promising prospect is photodiode arrays. Both Matsushita et al. (Matsushita et al. 1984b, Philzakerly et al. 1983) and Flank, Fontaine et al. (Flank et al. 1982, Dartyge et al. 1984) have successfully integrated photodiode arrays into their dispersive EXAFS systems. To minimize both noise and radiation damage,

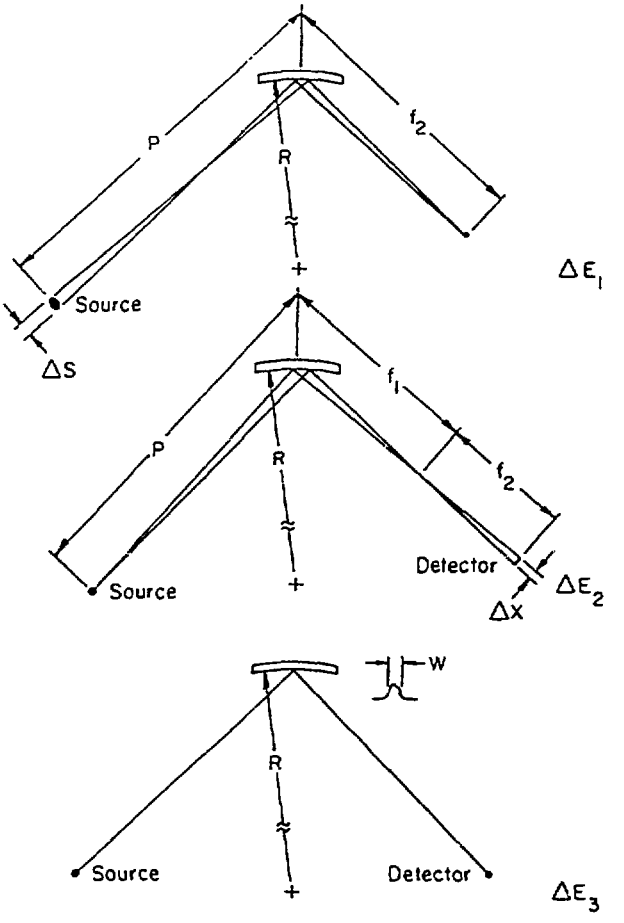

Fig. 14. The three contributions to the energy resolution of a dispersive X-ray absorption system are (a) source size, ΔS; (b) detector spatial resolution, ΔX; and (c) the intrinsic or Darwin width of the monochromating crystal, w (from Matsushita and Phizackerly 1981).

the arrays are normally cooled below room temperature. A thin layer of fluorescent material (GdO_2S or YVO_4:Eu) is normally deposited either directly on the device or onto the face of a fiber optic plate that is coupled to the array. Linear photodiode arrays are commercially available with 1024 pixels and a spatial resolution of 20–50 μm.

Recording the EXAFS spectra in this fashion has several inherent differences over the more conventional method that merit further attention. Care must be taken to insure that the sample thickness is uniform and that the X-ray beam is focused at the specimen, otherwise different wavelengths will sample different portions and/or thickness of the specimen. It is also important to realize that this system is intrinsically

a transmission technique. It may be limited to rather high-concentration samples, and applicable to more dilute samples only if many scans can be signal averaged.

Usable spectra of pure foils have been recorded in tens of milliseconds, consistent with the claim that for such foils energy dispersive methods should yield EXAFS curves of comparable statistics to conventional techniques in 10^{-4} the time (Phil-zakerly et al. 1983). For more dilute samples, timescales are naturally longer. Temporal resolutions of one second have been achieved with an 0.15 M Fe-solution in stop-flow cells with energy dispersive EXAFS systems (Matsushita et al. 1984b). As always, signal averaging can increase the temporal resolution. On a somewhat longer timescale, Sayers et al. (1984) have used this technique to measure the Pt L-edge of catalytic systems after exposure to hydrogen in a controlled environment furnace with samples containing 1% Pt by weight. Recently, time resolved in-situ measurements of the inclusion process of metallic aggregates in polymers have been reported (Tourillon et al. 1986).

3.3. Experiments utilizing the pulsed nature of synchrotron radiation

The best temporal resolution will be obtained by those experiments which utilize the pulsed nature of the beam. Experiments in this class, with temporal resolutions from 10^{-4} s to timescales commensurate with the pulse duration, require synchronization of external equipment to the X-ray pulses. Presently available synchrotron-radiation sources do not have the necessary brightness for adequate data to be collected from a single bunch, therefore, all experiments in this category must use regenerative perturbation techniques, i.e., repeated excitation/relaxation cycles. For those experiments that require large X-ray fluxes per pulse, it is important to realize that for a given average intensity, the power per pulse is inversely proportional with the number of bunches in the ring. Table 5 lists the calculated number of photons per burst and the instantaneous flux for several source points on the Advanced Photon Source (APS) to be constructed at Argonne National Laboratory. [Detailed information on the APS source properties can be found in Shenoy et al. (19??).]

Table 5

A list of the calculated number of photons per burst and the instantaneous flux for several source points on the APS. All calculations are made at the critical energy (for dipole and wiggler sources) or at the fundamental energy (for undulator) assuming 7.0 GeV 100 mA operation with 20 bunches. By adjusting the bandwidth of the monochromating system, large increases (10–100) in the number of photons per burst can be obtained with dipole and wiggler sources and to a lesser extent with undulator sources, since these have a natural line width of 1%.

Source	Number of photons per burst	Instantaneous flux
Dipole source	1.7×10^{6} p/0.1%BW mradθ	1.5×10^{16} p/s – 0.1%BW mradθ
Wiggler A	3.9×10^{7} p/0.1%BW mradθ	3.4×10^{17} p/s – 0.1%BW mradθ
Wiggler B	4.5×10^{7} p/0.1%BW mradθ	3.9×10^{17} p/s – 0.1%BW mradθ
Undulator A	2.1×10^{8} p/0.1%BW*	1.8×10^{18} p/s – 0.1%BW*
Undulator B	1.7×10^{8} p/0.1%BW*	1.5×10^{18} p/s – 0.1%BW*

*Integrated over the horizontal and vertical divergences of the central peak.

When the lifetime of the excited state is relatively long compared to the interpulse period of the X-rays, the X-ray pulses can be used to sample the excited state at precise intervals. This technique was used in a study carried out to investigate the possibility of extending time-resolved X-ray absorption spectroscopy to the submillisecond timescale. In this exploratory study, the recombination of ligands to the lone iron atom in the protein myoglobin was monitored by recording the X-ray absorption of the K-edge region of the iron atom as a function of time (Mills et al. 1984a, b). By observing the iron edge shape and position following ligand removal by laser photolysis, information on transient alterations in electronic and structural configurations that occur at the Fe atom were sought (fig. 15). Of particular interest were spectral features different from both the static deoxymyoglobin spectrum and the static carboxymyoglobin spectrum. In this preliminary investigation, the low repetition rate of the exciting laser (20 Hz) did not allow for sufficient signal averaging to obtain temporal resolution of the interpulse period ($\simeq 2.5$ μs). To obtain the data shown in fig. 15, it was necessary to add data collected from several X-ray pulses in order to obtain reasonable signal-to-noise ratios.

A particular problem that arises when working with biological materials is the possibility of damage to the sample either by the X-rays themselves or by the laser from the repeated excitation needed to collect the data. For solution samples, this problem can easily be remedied by using a flow cell in which the sample is continuously removed from the X-ray and laser beams, and replaced by new or recycled solution. Such a flow cell was used in the myoglobin experiment and is shown in fig. 16.

In the myoglobin experiment, as will be the case with many pump/probe experiments, the pump repetition rate must be weighed against the fraction of excited species produced. Often at low repetition rates the power per pulse of the pump is sufficient to excite nearly 100% of the sample, but signal averaging is slow due to the low pump rate. Conversely, the sample excitation rate can be increased, but generally at the expense of the percentage of excited species produced. An alternative approach is to maximize the pump repetition rate and to dilute the sample so that a large fraction of the sample can be excited even at the higher repetition rate. The price paid for sample dilution, of course, is a lower signal-to-noise ratio. All these issues must be considered when selecting pump power, pump repetition, sample size and concentration. For example, in the myoglobin experiment described above, the output of the frequency-doubled Nd:Yag laser used to excite the sample was $\simeq 3$ mJ per pulse, corresponding to $\simeq 10^{16}$ photons per pulse. With the flow-cell thickness of 0.1 cm and laser-beam cross section of 1×0.2 cm^2, the volume of sample illuminated by the laser was 2×10^{-2} cm^3. Near-complete photolysis of the myoglobin required a dilution of the sample to $\simeq 1$ mM. The cross-sectional area illuminated was determined in part by the minimum size of the X-ray beam that could be tolerated while still obtaining reasonable count-rates ($\simeq 0.6 \times 0.1$ cm^2). Focusing X-ray optical systems can decrease the X-ray size with little loss of flux. This means for a given power per pulse in the laser, the same number of excitable species can be contained in a smaller volume; in essence focusing optics permits an increase in the concentration of the sample with virtually no loss of excitation efficiency.

The results of the initial time-resolved spectroscopy studies are encouraging. Since the recombination time of the ligand to the myoglobin protein was $\simeq 1$ ms, a laser repetition rate of 20 Hz implies that only 2% of the time is the sample in an excited condition. Lasers are now available with 3 mJ/pulse and repetition rates of over 5 kHz. At such rates, future prospects for time-resolved XANES and EXAFS on a submillisecond regime are high.

The two time-resolved X-ray experiments that have achieved the best temporal resolution to date (nanoseconds) were performed under very different conditions. One experiment, devised by Larson et al. (1982, 1986) and shown schematically in fig. 17, set out to infer the temperature and temperature gradients in semiconducting materials following pulsed-laser annealing (fig. 18) by measuring the crystal reflectivity profile as a function of time. Three important experimental questions were addressed in this work:

(1) the synchronization of an external pump (laser) to the X-ray bursts;
(2) multiphoton counting techniques; and
(3) proper normalization procedures.

All of these are general problems that can arise in performing time-resolved experiments and so it is useful to examine at least one solution to each.

Synchronizing external equipment to emitted X-ray pulses requires some signal locked to the interpulse period. The cleanest signal is usually a clock-pulse signal from the RF system clock. Still, the relative arrival time of the X-rays with respect to the clock pulses needs to be established. This can be done with plastic scintillators attached to photomultiplier tubes if the transit time through the photomultiplier tube is well known. A much simplier technique is to use fast PIN photodiodes. Although generally not sensitive enough to be used in a monochromatic beam of X-rays without

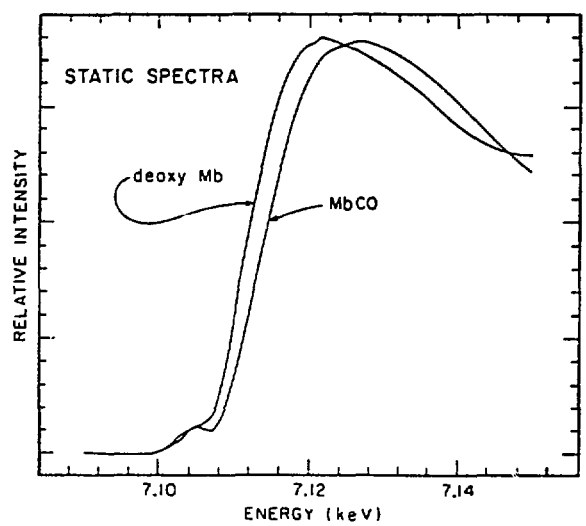

(a)

an amplifier, ample signal without electronic amplifiers can be obtained if there is a small portion of white beam available. These devices can provide a pulse signalling the arrival of the X-ray beam with very sharp risetimes (< 1 ns) and virtually no device propagation or transit time.

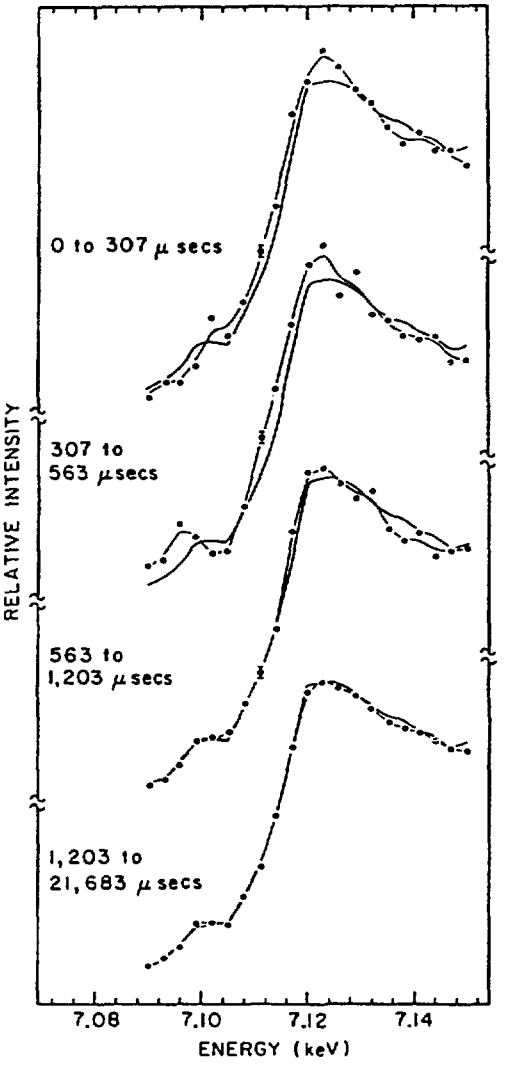

(*b*)

Fig. 15. X-ray absorption near-edge structure (XANES) as a function of X-ray energy for (a) carboxymyoglobin (MbCO) and deoxymyoglobin (deoxyMb) in a static state and (b) MbCO XANES spectra following laser-flash photodissociation of the ligand (CO) from the myoglobin protein. The solid line is the totally recombined MbCO spectrum and light lines are the time-resolved spectra. The times that the data were collected are shown on the left ($t = 0$ is the time the laser was fired). (Mills et al. 1984a.)

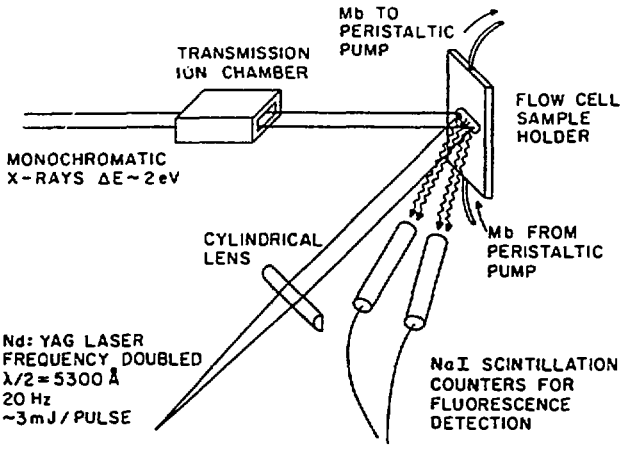

Fig. 16. Experimental arrangement under which the data of the previous figure was collected. The flow cell was used to minimize radiation damage of the sample from both the X-rays and the photolyzing laser light.

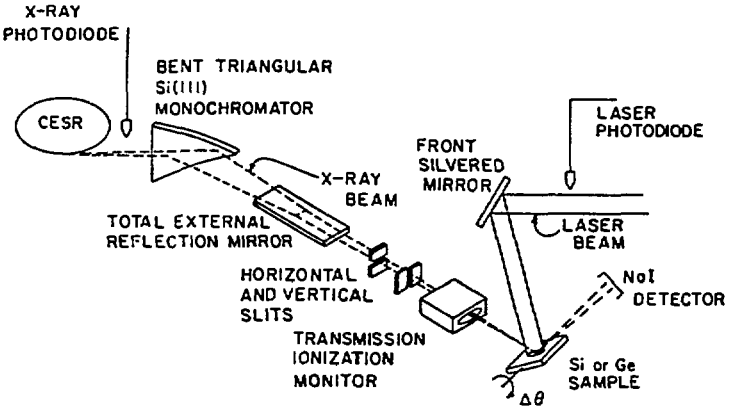

Fig. 17. Experimental geometry for the nanosecond resolved X-ray diffraction studies of pulse-laser annealed silicon. Because of the multiphoton counting technique used, a total-reflection X-ray mirror to remove unwanted higher harmonics for the Si(111) monochromator was a critical component. The sample reflectivity is measured for a given time between arrival of the laser and X-ray bursts (determined by the two photodiodes) as a function sample angle $\Delta\theta$, where $\Delta\theta = 0$ corresponds to the Bragg condition of the unperturbed sample.

Typically, several "ready" signals (laser ready, detector or interface ready) are input to a coincidence unit along with the storage-ring clock pulse. When all external equipment have asserted ready signals, the next storage-ring clock pulse will fire the coincidence unit output. The coincidence unit output, which is now synchronous with the clock pulse, initiates the laser firing sequence and the laser will fire at a given time with respect to the clock and hence X-ray pulse. A variable delay between the

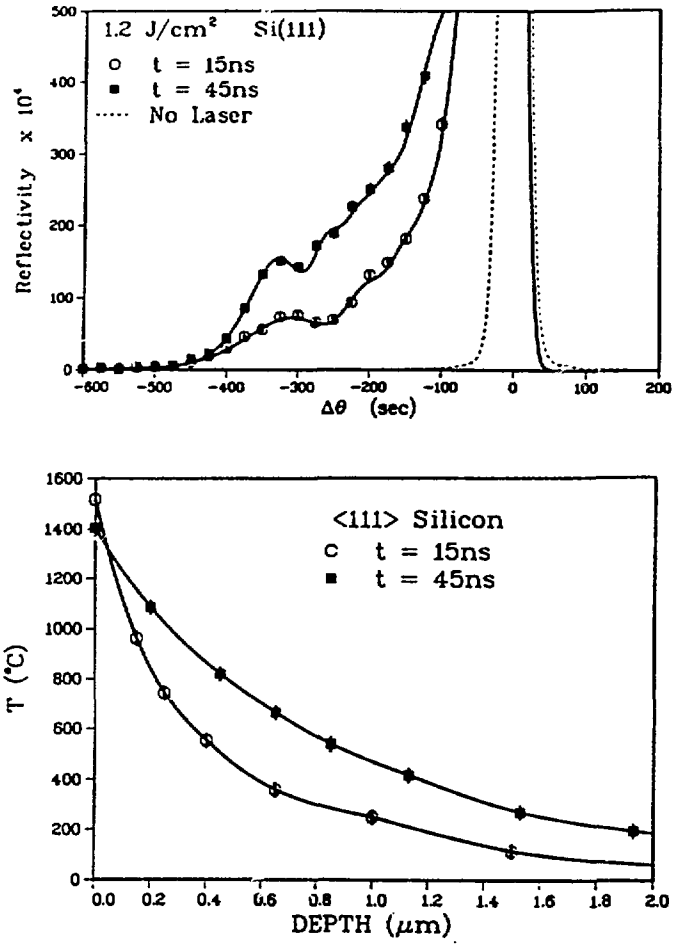

Fig. 18. In (a) reflectivity as a function of angle $\Delta\theta$ for Si(111) at two different times after the arrival of the annealing laser pulse are shown. In (b) the temperature profiles reconstructed from the reflectivity measurements are shown.

coincidence output and the external trigger of the laser provides the capability to vary the arrival time of the laser-light pulse with respect to the X-ray pulse. The coincidence unit output pulse is also used to gate counting electronics. The time between the laser and X-ray pulse can be recorded with a time to amplitude converter (TAC), e.g., if the laser output pulse is used for the start signal and the X-ray pulse is used for the stop input. Both asynchronous free-running lasers (Mills et al. 1984b) and externally controlled variable-rate lasers (Larson et al. 1986) can be synchronized in a similar fashion. Temporal resolutions of ± 2 ns were achieved in the experiment described above due to the jitter in the laser firing, not the storage-ring stability.

Both the short X-ray burst duration (160 ps FWHM) and the large number of monochromatic X-ray photons per burst (5×10^4) available at CHESS were advantageously used in the pulsed laser annealing investigation. It is convenient to have the duration of the probe beam much shorter than the timescales one wishes to investigate, in this case nanoseconds. However, the short burst duration was also used in a somewhat subtler way. With the laser repetition rate of only one per second, single-photon counting techniques would limit the maximum count rate available to one X-ray photon per second. In order that the data-collection time be minimized, a scheme was devised to perform multiphoton counting per bunch. The brief duration of each X-ray burst does not permit the proportional detectors used to discriminate multiple X-rays eminating from a single burst. Rather, when k photons per burst impinge upon a proportional-type detector, the detector output is not k pulses but rather one pulse with a height equivalent to k times that of an individual X-ray. Simultaneous photons (pulse pile-up) normally represents a complication to be avoided, however, in this case it is possible to take advantage of this effect to make quantitative scattering measurements using a single X-ray burst. Using standard pulse-height analysis techniques, the actual number of photons recorded from the burst is determined by comparing the multiple-photon pulse height to that of a single photon. Clearly, this type of analysis requires an X-ray beam well characterized in spectral content, i.e., having a minimum of harmonic contamination. Figure 19 shows the multiphoton effect in the pulse-height analyzed output from the detector displayed on a multichannel analyzer (MCA) for an actual count rate of $\simeq 2.5 \times 10^6$ photons/s,

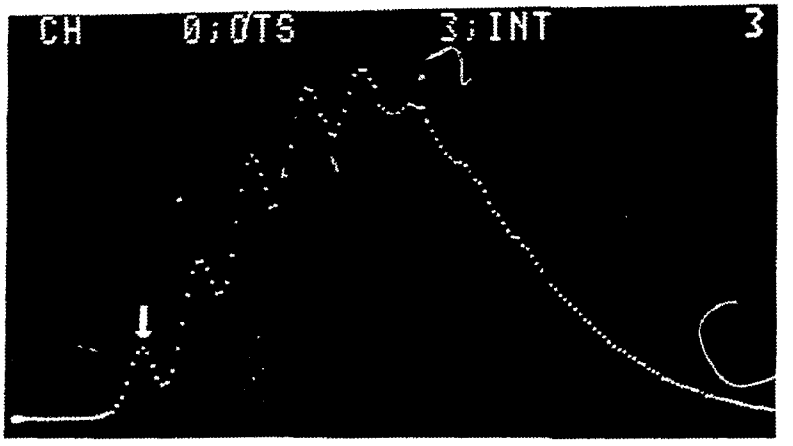

Fig. 19. The multichannel-analyzer (MCA) output intensity versus pulse height for a NaI scintillation detector exposed to a high count-rate monochromatic X-ray beam at CHESS. The arrow indicates the position of the peak corresponding to one photon per X-ray burst. The maximum of the MCA spectrum is near the peaks corresponding to 5 or 6 photons per burst being collected. Taking into account the interpulse period when this data was recorded (2.56 μs) this translates to a counting rate of 2–2.5 million X-ray photons per second incident on the detector.

i.e., an average of 6 X-ray photons per burst incident on the detector. (Data taken with CHESS running in single-bunch mode.) The multiple-photon events are clearly resolved. The maximum pile-up during data collection was limited to 15 X-ray photons per burst in order to remain in the linear range of the detector and associated electronics.

In order to compare measurements made over several days, some type of normalization is required. Normally, data are scaled by an ion chamber which monitors the average beam intensity. This method can also be used when making time-resolved measurements if only one bunch of particles is in the accelerator, since the ion-chamber output is directly proportional to the flux from that bunch. If there are multiple (p) bunches of particles in the storage ring there is no guarantee that each bunch will contain the same number of particles. Certain experimental circumstances could, however, give preference to one bunch with say a much lower than average number of particles over the others. In such a case, normalizing data with *average* beam intensity would lead to erroneous results. To circumvent this problem and still normalize to the average beam current, every datum point must be taken p times, each time advancing to a new bunch so that X-rays from *all the bunches are sampled at each data point.*

The second experiment to have achieved nanosecond resolution involved the use of stroboscopic topography (Gluer et al. 1983, Goddand et al. 1983). In this experiment, shown schematically in fig. 20, the sample was not excited once a second but rather at a harmonic of the repetition rate of the X-ray pulses (i.e., several megahertz). In this clever arrangement, fast detectors are not required since the system is prepared in its excited state every time the burst of X-rays impinge on it. By varying the relative phase between the pump and the X-ray bursts, the stroboscopic or time-frozen topographs can be produced at various times with respect to the excitation.

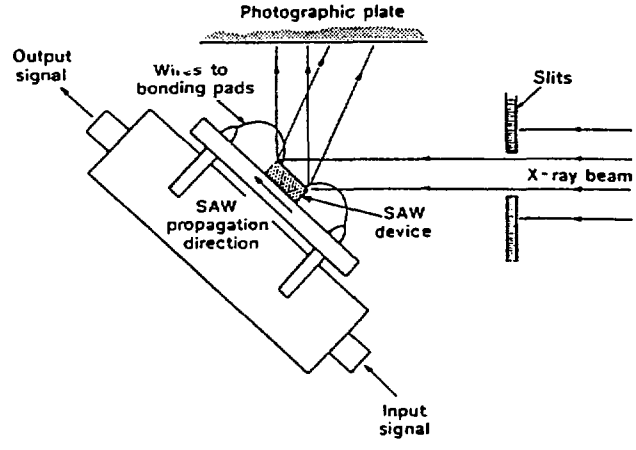

Fig. 20. Schematic representation of the experimental set-up used to record time-resolved X-ray topographs (Whatmore et al. 1982).

4. Future directions

In the experiments cited above, a wide variety of differing scientific disciplines have made use of time-resolved crystallographic, diffraction, topographic and spectroscopic techniques. The extension of static studies into a time-resolved regime in other X-ray fields such as Compton scattering, inelastic scattering and standing-wave investigations should be straightforward.

Well-developed methods in other fields may also be directly applicable to time-resolved X-ray studies. For example, the stroboscopic methods mentioned earlier are eminently suited to the high repetition rates available from storage-ring sources. By exciting the sample at some integer multiple of the repetition frequency of emitted radiation and systematically varying the relative phases between pump and probe, the entire time evolution of the transient phenomena can be mapped out. Using stroboscopic techniques, time-resolved data can be acquired not only in the same time as the equivalent data on a static sample, but without the need for high-speed detectors and data-acquisition systems. These methods have already been applied to one field of research, namely topography. Equally promising is the prospect of expanding stroboscopic techniques to other diffraction experiments allowing detailed studies of the dynamic behavior of a large class of systems in the megahertz to gigahertz frequency range. Similarly, by synchronizing amplified-mode-locked laser pulses to a repetition frequency of the X-ray pulses, stroboscopic spectroscopies including near-edge absorption spectra and EXAFS should be feasible.

Frequency domain or phase-shift methods (Gratten and Lopez-Delgado 1979, Rehn 1980) that have been developed for fluorescence-lifetime measurements with visible and ultra-violet synchrotron radiation may also be applicable to time-resolved X-ray studies. Calculations indicate that even with an incident burst several hundred picoseconds in duration, time resolution in the subpicosecond regime may be realized. A resolution level such as this, however, puts heavy demands on the stability of the storage-ring repetition frequency and consistency of the particle bunch shape.

Equipment development will play a crucial role in the future of time-resolved studies. New or improved machine-optics designs could allow very short pulse durations during special dedicated timing runs. Designers of the next generation of dedicated storage rings are hoping to achieve pulse lengths of several picoseconds under special running conditions. Short pulses, however, may severely limit the maximum amount of stored current and beam lifetime.

Inevitably, many of these time-resolved experiments will be "photon-hungry" experiments. Insertion device development (both wigglers and undulators) will certainly help to relieve this problem.

Developments in high speed, gated, one- and two-dimensional detectors need to be made. Fast phosphors and scintillators with a high quantum efficiency for X-ray down conversion will definitely be necessary along with more sophisticated multiphoton-counting capabilities.

In many instances, parallel improvements on many fronts will be necessary. For instance, insertion devices and energy dispersing monochromators used in conjunction with high speed, gateable, position-sensitive one-dimensional detectors may in

the future allow entire time-resolved EXAFS or near-edge spectra to be collected with nanosecond resolution in a total elapsed time of only a few seconds. Experiments in which the entire data set is produced by the X-rays emitted by a single bunch may be in store for the future. The calculated number of photons per burst from undulators being considered for the planned second-generation sources (Advanced Photon Source to be built in Argonne, IL, or the European Synchrotron Radiation Source to be built in Grenoble, France) is in excess of 10^8 X-rays/0.1% BW in the central peak of the radiation pattern. Construction of special insertion devices with broad (10%) harmonic peaks coupled with the appropriate wide-bandpass optics may allow one to put 10^{10} photons onto the sample from a single bunch. An even bolder consideration is to use a single bunch coupled with an X-ray streak camera to attempt experiments that subdivide the actual X-ray burst duration. New ideas such as these, along with the ingenuity of the varied community of users, will surely see the list of problems now being investigated with synchrotron radiation expanded to include transient phenomena.

Acknowledgements

The author would like to thank the many people that have graciously supplied preprints and reprints to be used in the writing of this manuscript. This work was begun while the author was at the Cornell High Energy Synchrotron Source (CHESS) and completed while on leave from CHESS at the Advanced Photon Source at Argonne National Laboratory. CHESS is funded by the NSF through grant DMR 84-12465. Support during the leave was provided by a fellowship from the John Simon Guggenheim Memorial Foundation and through DOE contract number W-31-109-ENG-38.

References